RI 7908

BuMines RI 7908

PB240666

Bureau of Mines Report of Investigations/1974

Mathematical Study of a Propagating Flame and Its Induced Aerodynamics in a Coal Mine Passageway

UNITED STATES DEPARTMENT OF THE INTERIOR

T_b = T on the burned side of the flame front.

T_w = Wall temperature (K).

t = Time (sec).

τ_{xy} = Shearing stress (kg m^{-1} sec^{-2}).

τ_{xz} = Shearing stress (kg m^{-1} sec^{-2}).

τ_w = Shearing stress at the wall (kg m^{-1} sec^{-2}).

μ = Viscosity (kg m^{-1} sec^{-1}).

u = Velocity in the longitudinal direction or the x-component of the velocity vector $\overline{w}$ (m sec^{-1}).

u_b = u on the burned side.

u_u = u on the unburned side.

v = y-component of the velocity vector $\overline{w}$ (m sec^{-1}).

w = z-component of the velocity vector $\overline{w}$.

n = Position (1).

xF^t = Location of flame front at time t (m).

$xF^{t+\Delta t}$ = Location of flame front at time $(t + \Delta t)$.

Report of Investigations 7908

Mathematical Study of a Propagating Flame and Its Induced Aerodynamics in a Coal Mine Passageway

By Donald N. H. Chi and Henry E. Perlee
Pittsburgh Mining and Safety Research Center, Pittsburgh, Pa.

UNITED STATES DEPARTMENT OF THE INTERIOR
Rogers C. B. Morton, Secretary

BUREAU OF MINES
Thomas V. Falkie, Director

This publication has been cataloged as follows:

Chi, Donald N H

Mathematical study of a propagating flame and its induced aerodynamics in a coal mine passageway, by Donald N. H. Chi and Henry E. Perlee. [Washington] U.S. Bureau of Mines [1974]

51 p. illus. (U.S. Bureau of Mines. Report of investigations 7908)

Includes bibliography.

1. Flame. 2. Coal mines and mining--Safety measures. I. Mine fires. II. Perlee, Henry E., jt. auth. III. U.S. Bureau of Mines. IV. Title. (Series)

TN23.U7 no. 7908 622.06173

U.S. Dept. of the Int. Library

CONTENTS

ILLUSTRATIONS

ILLUSTRATIONS--Continued

MATHEMATICAL STUDY OF A PROPAGATING FLAME AND ITS INDUCED AERODYNAMICS IN A COAL MINE PASSAGEWAY

by

Donald N. H. Chi[1] and Henry E. Perlee[2]

ABSTRACT

The unsteady, one-dimensional, compressible-flow equations have been solved numerically for a deflagration propagating through a gallery of finite length closed at the ignition end and open at the opposite end. These equations were solved for two situations wherein (1) the propagating flame was extinguished after 0.1 sec or before the return of aerodynamic disturbances reflected from the open end, and (2) the flame was allowed to propagate a full 0.8 sec until it was extinguished. It was found that the process of sudden flame extinguishment creates rarefaction waves that, upon entering the burned zone, produce resonance within the burned cavity. For the relatively small value of the product of the expansion ratio (8.5) and the effective burning velocities of 7.4 m sec^{-1} for the first experiment and 4.9 m sec^{-1} for the second experiment, it was found that the acoustic approximation provides an adequate estimate of the pressures developed ahead of the flame during the system's early history.

INTRODUCTION

Background Information

This study was undertaken as a continuation of the Bureau of Mines effort to conduct mathematical investigations of the aerodynamic history of flames (deflagrations) propagating through flammable gas mixtures in coal mine passageways using a one-dimensional, transient, compressible-flow description. The initial Bureau effort (13)[3] dealt with the history of flame-induced aerodynamic disturbances ahead of a flame front where the flow was assumed isentropic and the flame history was an implicit function. That study was concerned exclusively with the aerodynamics of the unburned gas region and neglected the possible creation of shocks. Although this approach severely limited the range of applications, it found its major use in extending experimentally measured variable histories to uninstrumented regions. (See

[1] Research physicist.

[2] Supervisory research chemist.

[3] Underlined numbers in parentheses refer to items in the bibliography preceding the appendixes.

reference 13 for a more complete discussion of this application.) Although it was found that the calculated pressure history agreed with the experimentally measured values to within 10 percent, it was felt that the calculations had to be extended to include the burned region to study the interaction between the flame front and its induced aerodynamics. Furthermore, although the method of characteristics was useful for solving the equations in this earlier study, it proved to be cumbersome in dealing with both the flame front and the shocks.

The alternate approach consists of using the modified Lax-Wendroff scheme (29) proposed by Rubin and Burstein (42) for solving the descriptive finite difference equations. Through the use of this technique it is no longer necessary to keep track of the shock trajectories since the algorithm deals with these explicitly. However, the flame is treated as a moving, internal boundary, not explicitly handled by the finite-difference equations. The resulting computer program is very flexible and useful for parametric studies.

To test this code, the Bureau of Mines examined two flame propagation situations in a 50-meter long, smooth-walled gallery with a radius of 0.69 meter. For the first part of the study, a flame propagated from the closed end with a constant velocity for a period of 0.1 second after which it was suddenly quenched creating a contact surface at the flame-front location. The research examined mathematically the interactions between the contact surface and the flame induced aerodynamics. In the second phase of the study, the flame was allowed to continue propagating until it self-extinguished, its interactions with the induced aerodynamic disturbances was examined. The results of these two studies have been useful in the interpretation of experimentally measured histories in both laboratory-scale galleries and the Bureau's Experimental Coal Mine.

Historical Development

Jones (26) reported work which is very much in the spirit of the present work in which he obtained analytical solutions of linearized equations and studied the aerodynamics ahead of accelerating flames. In his studies the flame front was treated as a plane of discontinuity, moving with a prescribed acceleration. The energy that sustains this acceleration is then computed a priori. The limitation of this model lies in the fact that acceleration of the flame is fixed and consequently unaffected by its interaction with the induced aerodynamic disturbances.

In the subsequent work of Artingstall (5-6) concerned with the propagation of coal-dust explosions, the author assumes that the system has attained a steady state. To deal with the unsteady state he applies the method of wave diagrams (see Rudinger (43)) to the flow equations. Such techniques are useful but they become rather cumbersome in keeping track of the wave interactions.

Markstein (33) suggested that the flame may be treated as an internally moving boundary, across which the phenomenological variables, burning velocity Su and expansion ratio χ, define the combustion process. This procedure avoided having to deal with the mathematically cumbersome description of the

flame structure concerned with chemical kinetics and transport processes. This paper has adopted Markstein's proposition although his assumption of incompressible flow will be removed.

ACKNOWLEDGMENTS

Our sincere thanks go to Israel Liebman, Kenneth J. Richmond, and Joseph M. Singer for their helpful suggestions and numerous discussions illuminating the combustion phenomena in flame galleries and in the Experimental Mine of the Pittsburgh Mining and Safety Research Center.

THE MODEL

The physical problem that this paper proposes solving involves the one-dimensional propagation of a deflagration through a cylindrical gallery closed at the ignition end and open at the other end. Two alternative methods exist for dealing with the deflagration. One involves the inclusion of appropriate terms in a basic conservation equation to account for thermal transport and exothermic reactions. In this manner the deflagration becomes an implicit part of the partial differential equation and the equations can be solved by spatial integration between the two ends of the gallery. Unfortunately neither the one-dimensional nature of the transport mechanisms nor the functional nature of the exothermic reaction are readily available; hence, such an approach requires considerable speculation on the part of the investigator and consequently, the results lack rigor. The second approach, that adopted in this study, uses two experimentally measurable quantities, the expansion ratio and the burning velocity, to define the deflagration characteristics appropriate to its aerodynamic response. These two parameters provide all the necessary physical information required to completely characterize the aerodynamic characteristics of the deflagration process. However, since χ and Su are not implicitly contained within the partial differential equations, one is necessarily required to use separate sets of partial differential equations to characterize the burned and unburned regions and to match their solutions at the flame front using boundary conditions appropriate to a deflagration. These boundary conditions which include Su and χ will be introduced at a later point in this paper.

Assumptions

The following simplifying assumptions will be adopted to facilitate solution of the problem:

1. The flow is quasi-one-dimensional in the sense that the field variables (pressure, velocity, temperature, density, energy, entropy, etc.) represent averages over the cross sectional area, and the field components in the transverse direction are neglected compared with those in the longitudinal direction.

2. The gas is homogeneous and continuous except across the flame front.

3. The gas is always in thermodynamic equilibrium; that is, its thermodynamic state is uniquely determined by any two independent state variables.

4. Body forces are neglected.

5. The gas obeys the ideal-gas law.

6. Molecular transport phenomena such as heat conduction and mass diffusion are neglected.

7. Radiant transport is neglected.

8. The shearing stresses $\tau_{xy} = \mu \frac{\partial u}{\partial y}$ and $\tau_{xz} = \mu \frac{\partial u}{\partial z}$ at the wall are constant at any cross section and the normal viscous stress $\mu \frac{\partial^2 u}{\partial x^2}$ is negligible compared to τ_{xy} and τ_{xz}.

9. The flame front is treated as an internal moving boundary across which the flow fields are discontinuous. The two phenomenological variables, namely, the expansion ratio χ and the burning velocity Su completely characterize the flame.

It has been observed (see Liebman (31) and Laderman and Oppenheim (28)) that the flow fields at a cross section of flame gallery are fairly uniform except within a distance of a few centimeters from the wall. This theory lends justification to the use of a one-dimensional model. The body forces, such as gravitational force, can, if necessary, be included in the model without much difficulty and the ideal-gas assumption is not a restriction to the numerical solution.

Studies in the flame gallery show that the flame augments the intensity of turbulence, which in turn accelerates combustion in the flame. Although the initial study is restricted to laminar flow, turbulent effects can be included through the phenomenological expressions. The simplest treatment is to consider a turbulent flame as a "laminar flame with a pleated surface." This implies that we may replace the laminar burning velocity Su by a turbulent burning velocity or by an effective burning velocity $Su^{\dagger}$. It is evident from the experimental data that laminar burning velocity cannot explain the flame speed observed.

Governing Equations

In reference 13 the derivation of the following conservation laws that govern the flow fields away from the boundaries is given:

1. Conservation of mass

$$\frac{D\rho}{Dt} + \rho \frac{\partial u}{\partial x} = 0 \tag{1}$$

where $$\frac{D}{Dt} = \frac{\partial}{\partial t} + u \frac{\partial}{\partial x}$$

(the substantive derivative);

2. Conservation of momentum

$$\frac{Du}{Dt} + \frac{1}{\rho} \frac{\partial P}{\partial x} + F = 0 \tag{2}$$

where $$F = \frac{4 \cdot f}{D} \cdot \frac{u^2}{2} \cdot \frac{u}{|u|} \tag{3}$$

and $$f = 0.0014 + 0.125 \cdot (Re)^{-0.32} \quad \text{for } 3 < Re < 3 \times 10^6 \tag{4}$$

where f is the friction factor for smooth wall.

3. Conservation of energy

$$\frac{D}{Dt}\left(e + \frac{u^2}{2} \right) = q - \frac{u}{\rho} \frac{\partial P}{\partial x} - \frac{P}{\rho} \frac{\partial u}{\partial x} . \tag{5}$$

Finally, we need the equation of state to form a closed system; hence,

$$P = \rho \cdot R \cdot T \text{ or } P = (\gamma - 1) \cdot \rho \cdot e . \tag{6}$$

Since these partial differential equations of gas dynamics are based on conservation laws, it is highly desirable to preserve these conservative properties in the finite difference equation. This is achieved, as shown by Courant and Friedrichs (14), by using the following transformations:

$$m = \rho \cdot u \qquad \text{(mass flux)} \tag{7}$$

and $$E = \rho(\tfrac{1}{2}u^2 + e) \qquad \text{(total energy per unit volume).} \tag{8}$$

The governing equations 1, 2, and 5 can now be written as (see appendix A for the mathematical details):

$$\frac{\partial \rho}{\partial t} = - \frac{\partial m}{\partial x} \tag{9}$$

$$\frac{\partial m}{\partial t} = - \frac{\partial}{\partial x}\left(\frac{m^2}{\rho} + P \right) - \rho \cdot F \tag{10}$$

and $$\frac{\partial E}{\partial t} = - \frac{\partial}{\partial x}\left[\frac{m}{\rho} (E + P) \right] + \rho \cdot q . \tag{11}$$

Furthermore, if $\overline{w}$ is defined to be the vector

$$\overline{w} = \begin{bmatrix} \rho \\ m \\ E \end{bmatrix},$$

and $\overline{f}(\overline{w})$ and $\overline{g}(\overline{w})$ are defined as the vector-valued functions

$$\overline{f}(\overline{w}) = \begin{bmatrix} -m \\ -\left(\frac{m^2}{\rho} + P\right) \\ -\frac{m^2}{\rho}(E+P) \end{bmatrix} \text{ and } \overline{g}(\overline{w}) = \begin{bmatrix} 0 \\ -\rho \cdot F \\ -\rho \cdot q \end{bmatrix}$$

Thus, the system of equations 9 to 11 can be expressed in the form

$$\frac{\partial \overline{w}}{\partial t} = \frac{\partial \overline{f}}{\partial x} + \overline{g} \ . \qquad (12)^4$$

Such a form is referred to as conservation-law form. It can be readily shown that retaining this form in the finite difference equations, the conservation of mass, momentum, and energy is maintained across a mesh. This is an important characteristic of the finite difference equation, since the Rankine-Hugoniot relations across a normal shock are macroscopic conservation laws not involving the microscopic shock structure. This conservative property of the finite difference equation guarantees satisfaction of the Rankine-Hugoniot relations and therefore the correct jump conditions across a shock front. Consequently, there is no need to treat the shock separately outside the difference equations as an internal moving boundary, since the finite difference equations can handle the shock implicitly. In terms of mathematical terminology, such finite difference methods will yield a weak solution, one in which discontinuities can occur or differentiability can be isolated. Note that the finite difference analogue of the partial differential equations written in conservation-law form can be interpreted as an integral law over each mesh, which can be thought of as a control volume.

Boundary Conditions

For the specific problem of interest to this investigation the following boundary conditions are required:

1. At the closed-end (x=0)

$$u(0,t) = 0 \ ;$$

---

[4]Note that μ does not appear explicitly in the energy equation. See appendix G for more details.

2. at the open-end (x=Lt)

$$P(Lt,t) = P_o$$

where Lt is the length of the gallery and P_o is the ambient pressure;

3. across the flame front we use the following conservation laws where the subscripts u and b denote the flow fields on the unburned and the burned sides, respectively, and S_u and S_b denote the unburned and burned gas velocities relative to the flame front, respectively.

From the conservation of mass we obtain the expression,

$$\rho_u S_u = \rho_b S_b \text{ at } x=x_f \tag{13}$$

while the conservation of momentum provides

$$P_u - P_b = \rho_b S_b^2 - \rho_u S_u^2 \text{ at } x=x_f . \tag{14}$$

Instead of the energy conservation law which requires knowledge of the chemical kinetics we used the expansion ratio,

$$\chi = \rho_u / \rho_b , \text{ at } x=x_f$$

to relate the gas densities on either side of the flame front.

By using the definition of flame speed $S_F = u_u + S_u$ or $S_F = u_b + S_b$, the definition of sound speed $(c_b = \gamma_b R_b T_b)^{\frac{1}{2}}$ and the equations of state $P_u = \rho_u R_u T_u$ and $P_b = \rho_b R_b T_b$, we reduce the above boundary conditions to

$$\rho_u = \chi \rho_b , \tag{15}$$

$$u_u = u_b + (\chi-1) S_u , \tag{16}$$

and

$$P_u = P_b \left[1+\gamma_b \cdot \chi(\chi-1) \left(\frac{S_u}{c_b} \right)^2 \right] . \tag{17}$$

All these expressions are evaluated at $x = x_f$. $T_b(x = x_f)$ and χ are obtained from chemical equilibrium calculations and are implicitly a function of $P_u(x = x_f)$ and $T_u(x = x_f)$.

If the flame is extinguished at any time, our flame front discontinuity becomes a contact discontinuity in which case the above three conditions are replaced by

$$u_u = u_b , \tag{18}$$

$$P_u = P_b , \tag{19}$$

$$\rho_u = P_u^{1/\gamma_u} \text{ and } \rho_b = P_b^{1/\gamma_b} . \tag{20}$$

To complete our model we used the following initial conditions:

On the burned side of the flame front $u = 0$, $T = T_b$, $P = P_o$, and $\rho = \rho_b$ for $x = 0$ and $t = 0$; and

on the unburned side $u = (\chi - 1)S_u$, $P = P_o$, $T = T_o$, and $\rho = \rho_o$ at $x = 0$ and $t = 0$.

Elsewhere all flow fields are equal to their ambient quantities and $u(x, 0) = 0$, $x > 0$.

Equations of the Characteristics

As we shall see later, we use the method of characteristic to relate the flow fields at the boundaries to those of neighboring points in both the burned and unburned regions. For this reason we need to derive the appropriate characteristic equations. It can be shown (14, 45) that equations 1, 2, and 3 are equivalent to the following set of ordinary differential equations:

$$\frac{du}{dt} + \frac{1}{\rho \cdot c}\frac{dP}{dt} = (\gamma-1)\frac{q}{c} - F\left[1-(\gamma-1)\frac{u}{c}\right], \tag{21}$$

$$\frac{dx}{dt} = u + c, \tag{22}$$

$$\frac{du}{dt} - \frac{1}{\rho \cdot c}\frac{dP}{dt} = -(\gamma-1)\frac{q}{c} - F\left[1+(\gamma-1)\frac{u}{c}\right], \tag{23}$$

$$\frac{dx}{dt} = u - c, \tag{24}$$

$$\frac{dP}{dt} - c^2\frac{d\rho}{dt} = (\gamma-1)\cdot\rho\cdot(q+uF), \tag{25}$$

and finally

$$\frac{dx}{dt} = u. \tag{26}$$

We hasten to point out that the solution of equations 21, 23, and 25 are the two characteristic curves C_+ and C_-, and the particle trajectory C_g, respectively. Moreover, equations 21, 23, and 25 are valid only along their respective characteristics, namely, the curves

C_+ which is given by $x_+ = \int_{t_1}^{t} (u+c)dt$,

C_- which is given by $x_- = \int_{t_1}^{t} (u-c)dt$,

and

C_g which is given by $x_p = \int_{t_1}^{t} udt$.

$$\frac{\partial}{\partial t}\begin{bmatrix}\rho\\ m\\ E\end{bmatrix} = \frac{\partial}{\partial x}\begin{bmatrix}-m\\ -(m^2/\rho+P)\\ -m(E+P)/\rho\end{bmatrix} + \begin{bmatrix}0\\ -\rho\cdot F\\ -\rho\cdot q\end{bmatrix}$$

and

$$\frac{dx_f}{dt} = u_u(x,t) + S_u(x,t) \tag{27}$$

over both the burned and unburned regions satisfying the boundary conditions

$$\rho_u = \chi\rho_b \ ,$$

$$u_u = u_b + (\chi-1)S_u \ ,$$

and

$$P_u = P_b\left[1+\gamma_b\cdot\chi(\chi-1)\cdot\left(\frac{S_u}{c_b}\right)^2\right]$$

across the flame front; however, we use $u_u = u_b$, $P_u = P_b$, $\rho_u = P_u^{1/\gamma_u}$, and and $\rho_b = P_b^{1/\gamma_b}$ across the contact surface and $u(0, t) = 0$ and $P(Lt, t) = P_o$ at the two ends of the gallery. The method of characteristics was used to match the boundary conditions to the partial differential equations at the boundaries.

System Parameters

As we have already seen, the system is dependent on the five functional parameters S_u, χ, T_b, γ_u, and γ_b. Three of these parameters namely χ, T_b, and γ_b are calculated from the Gordon and McBride (19) Chemical Equilibrium Combustion Program for various values of pressure and unburned gas temperature for a homogeneous stoichiometric methane-air mixture. γ_u is calculated from values of γ for the reactants (air and methane) using the JANAF tables (25). These calculated quantities (ρ_b, T_b, γ_b, and γ_u) are regressed against the pressure and unburned gas temperature to obtain the following expressions:

$$\gamma_u = 1.3900 + 2.454 \times 10^{-4}\ T_u - 7.721 \times 10^{-7}\ T_u^2 + 4.83 \times 10^{-10}\ T_u^3 \tag{28}$$

where T_u is in Kelvin;

$$\gamma_b = 1.2005 + 5.038 \times 10^{-3}\ P_u - 2.6515 \times 10^{-4}\cdot P_u^2 - 6.07 \times 10^{-5}\ T_u \tag{29}$$

where P_u is in atm;

$$\rho_b = 10^{-3} \times (8.7694 \times 10^{-3} + 1.59487 \times 10^{-1} P_u - 3.56567 \times 10^{-5} T_u - 1.012662 \times 10^{-6} P_u^2 - 3.57939 \times 10^{-5} T_u \cdot P_u + 4.56762 \times 10^{-8} \cdot T_u^2) \quad (30)$$

in (gm cm^{-3});

and

$$T_b = [8.81553 \times 10^6 + P_u (3.74301 \times 10^6 + 1.63201 \times 10^3 \cdot T_u + 1.70406 \times 10^3 T_u]/[4.23302 \times 10^3 + P_u (1.78149 \times 10^3 + 2.27219 \times 10^{-1} T_u) - 1.66715 \times 10^{-2} T_u] . \quad (31)$$

The laminar burning velocity for a homogeneous unburned mixture, which is a function of the pressure and unburned gas temperature at the flame front can, at present, only be obtained from experiments. However, for the purpose of this preliminary investigation, two particular functional forms will be used to simulate constant burning, and constant burning followed by sudden flame extinguishment. The particular forms will be introduced in the discussion of the cases.

COMPUTATIONAL PROCEDURE

To arrive at a finite-difference analogue of the system of equation 27 or its equivalent equations 21 through 26, the space domain is divided into equidistant mesh points $\{x_i \mid i = 1,2, --, N + 1, x_{i+1} = x_i + (i - 1)\Delta x\}$ separated by an interval Δx.

Since the algorithm used to solve the finite difference equations requires a set of three nodal points, special consideration has to be given to the situation when the flame front is within two nodal points of the boundaries. If the flame is within two nodal points of the closed end, this is designated as category one; if it is within two nodal points of the open end, this is category three; and if the flame is anywhere else, the designation is category two. The algorithm used to compute the flow fields at each nodal point depends on the location of the flame front. At nodes at least at a distance of 2 Δx away from the boundaries, a modified Lax Wendroff algorithm (42) is used to solve equation 27. At the open end, closed end, and across the flame front, a first order finite difference analogue of the characteristic equations 21 through 26 is used. For nodal points adjacent to the flame, linear interpolation is used to calculate the field variable from their values on the flame front. Method of lines has also been used at these locations.

Depending on the three categories and the direction of travel of the flame, there are 42 separate cases that must be considered in order to solve the equations in the vicinity of the flame front. Appendix C gives a detailed listing of all 42 cases.

Modified Two-Step Lax-Wendroff Scheme

Recall that the system of partial differential equations 9 through 11 can be written in the form

$$\frac{\partial \bar{w}}{\partial t} = \frac{\partial \bar{f}}{\partial x} + \bar{g}$$

or

$$\bar{w}_t = \bar{f}_x(\bar{w}) + \bar{g}(\bar{w})$$

where $\bar{w}$, $\bar{f}$, and $\bar{g}$ are vector-valued functions defined in the section on "Governing Equations." In the following discussion we omit the term $\bar{g}(\bar{w})$ and examine one component of equation 12; thus, the bars above all the variables will be removed. The Lax-Wendroff scheme is based on a Taylor series expansion of the function $w(t+\Delta t)$ where the second order term w_{tt} in the expansion is replaced by the expression

$$w_{tt} = (f_x)_t = (f_t)_x = (Aw_t)_x = (Af_x)_x \quad , \tag{33}$$

where A is a matrix whose determinant is the Jacobian of f(w) with respect to w. Thus, an approximate value for $w(x+\Delta x, t+\Delta t)$ is given by

$$w_n^{t+\Delta t} = w_n^t + \frac{\Delta t}{2\cdot\Delta x}\left[f_{n+1}^t - f_{n-1}^t\right] + \frac{1}{4}\left(\frac{\Delta t}{\Delta x}\right)^2 \cdot$$

$$\left[(A_{n+1} + A_n)(f_{n+1}^t - f_n^t) - (A_n + A_{n-1})(f_n^t - f_{n-1}^t)\right] \tag{34}$$

where w_n^t, f_{n+1}^t, and f_{n-1}^t designate $w(x+n\Delta x,t)$, $f(x+(n+1)\Delta x,t)$, and $f(x+(n-1)\Delta x,t)$.

Richtmyer (41) used the same procedure to obtain a two-step Lax-Wendroff scheme with an overall accuracy of second order. Rubin and Burstein (42) modified the Richtmyer algorithm and arrived at the following algorithms:

$$w_{n+\frac{1}{2}}^{t+\Delta t} = \frac{(w_{n+1}^t + w_n^t)}{2} + \left(\frac{\Delta t}{\Delta x}\right)(f_{n+1}^t - f_n^t) \quad , \tag{35}$$

and

$$w_n^{t+\Delta t} = w_n^t + \left(\frac{\Delta t}{2\cdot\Delta x}\right)\left[\frac{f_{n+1}^t - f_{n-1}^t}{2} + f_{n+\frac{1}{2}}^{t+\Delta t} - f_{n-\frac{1}{2}}^{t+\Delta t}\right] . \tag{36}$$

To find $w_n^{t+\Delta t}$, one proceeds as follows: Compute $w_{n+\frac{1}{2}}^{t+\Delta t}$ and $w_{n-\frac{1}{2}}^{t+\Delta t}$ by using equation 35, evaluate $\bar{f}(\bar{w})$ at these two points and substitute these values into equation 36, along with the corresponding values at the points $((n-1)\Delta x,t)$, $(n\Delta x,t)$, and $((n+1)\Delta x,t)$. It is clear that whenever the flame front trajectory lies within the interval $((n-1)\Delta x,(n+1)\Delta x)$ the present procedure is no longer applicable and special treatment is required. Rubin and Burstein (42) have shown that the Lax-Wendroff, the Richtmyer-Lax-Wendroff, and the Burstein-Lax-Wendroff all have the same amplification matrix (40). This

implies that they all have the same stability criteria, namely, the Courant-Friedrichs-Lewy (15) stability condition,

$$\Delta t \leq \frac{\Delta x}{|u|+c}$$

where c and u are the local sound speed and gas velocity, respectively. For the detailed proof, see the work of Lax and Wendroff (29). Rubin and Burstein have also shown in (42) that their approach seems to be the best of the three in minimizing overshoot near the tail of shocks.

If we include the g term in the original equation, we add a term $\Delta t \cdot g^t_{n+\frac{1}{2}}$ and $\Delta t \cdot g^t_n$ to obtain the final form

$$w^{t+\Delta t}_{n+\frac{1}{2}} = \frac{(w^t_{n+1} + w^t_n)}{2} + \left(\frac{\Delta t}{\Delta x}\right)(f^t_{n+1} - f^t_n) + \frac{\Delta t}{2}(g^t_n + g^t_{n+1}) \qquad (37)$$

and

$$w^{t+\ t}_n = w^t_n + \frac{\Delta t}{2 \cdot \Delta x}\left(\frac{f^t_{n+1} - f^t_{n-1}}{2} + f^{t+\Delta t}_{n+\frac{1}{2}} - f^{t+\Delta t}_{n-\frac{1}{2}}\right) + \Delta t \cdot g^t_n \ . \qquad (38)$$

The addition of these terms does not alter the stability criteria since the amplification matrix is not affected. Appendix E contains the equations 37 and 38 into their nondimentional component forms.

Method of Characteristics

To compute the flow fields on both sides of the flame front, the method of characteristics was used in conjunction with the deflagration boundary conditions. Figure 1 shows the intersection of four curves, the flame (or contact surface) trajectory (C_f), the particle trajectory (C_g), and the two characteristics C_+ and C_-.

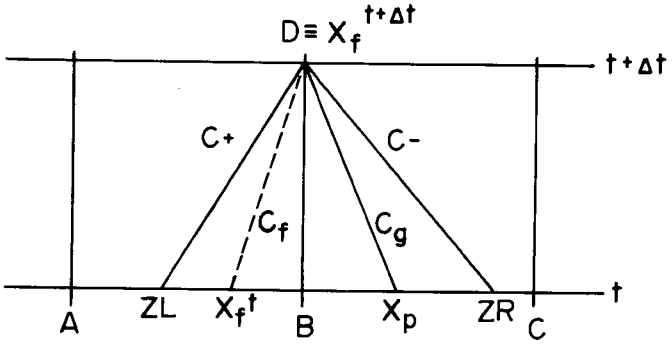

FIGURE 1. - The characteristic curves at the flame front.

In figure 1, x^t_f and $x^{t+\Delta t}_f$ are the location of flame front at time t and $t+\Delta t$, respectively. When the finite difference analogue of the system of equations 21 through 26 is used in conjunction with the boundary conditions equations 15 through 17, the final working equations are obtained. (See appendix E for details.) When the flame front is within the zone adjacent to the

closed (open) boundary special treatment is required since $C_-(C_+)$ intersects the boundary. This treatment is included in appendix E. Note that since the flame loci, the particle trajectory, and the C_+ characteristic curve are given by the solution of the equations

$$\frac{dx_f}{dt} = u_u + S_u , \quad \frac{dx_p}{dt} = u_p , \text{ and } \frac{dx_{c_+}}{dt} = u + c_+ ,$$

respectively, the particle trajectory always lies between the flame loci and C_+. This fact simplifies considerably the computational effort. A flow chart of the program structure is shown in appendix F.

RESULTS AND DISCUSSION

In this section the mathematics developed in the previous sections are used to study the aerodynamic history associated with a flame propagating along a 50-meter-long, 0.69-m-diameter smooth-walled gallery containing a stoichiometric methane air mixture. It is the particular purpose of this initial study to examine the interaction of the flame-induced aerodynamics with (1) the flame front (phase 1) or (2) the contact surface formed following flame extinguishment (phase 2). To facilitate the analysis we have chosen burning velocity as constant and equal to 7.4 m sec^{-1} although the remaining parameter functions (γ_u, γ_b, E, and C) are specific to a stoichiometric methane/air mixture.

In this preliminary study we do not strive to obtain accurate estimates of system histories as measured experimentally. It is more the purpose to identify and study the major aerodynamic characteristics associated with deflagrations propagating in coal mine passageways.

In the following sections two combustion processes are considered, both characterized by a constant burning velocity and an expansion ratio given by $\chi = \rho_u / \rho_b$ where ρ_b is given by equation 30.

Interaction With Contact Surface (Phase 1)

In the first phase of this study the full set of partial differential equations given in the section on "Governing Equations" were solved for a flame propagating at a constant burning velocity of 7.4 m sec^{-1} for a duration of 0.1 sec, after which $S_u = 0$ and a contact surface replaces the flame front. This value of 7.4 m sec^{-1} was chosen because it results in the same peak pressures ahead of the flame front as measured in the 50-meter gallery. A burn duration of 0.1 sec was chosen to insure that the leading edge of the aerodynamic pulse traveling ahead of the flame and reflected from the open end had not yet returned to the flame before the flame extinguishes. Solution of this problem for a real time of 0.5 sec required about 6.5 min of computer time on a CDC 6500.

Figures 2 and 3 show the calculated pressure and velocity histories at locations 0, 2, 4, 6, 8, and 10 m from the ignition. Figures 4 and 5 show

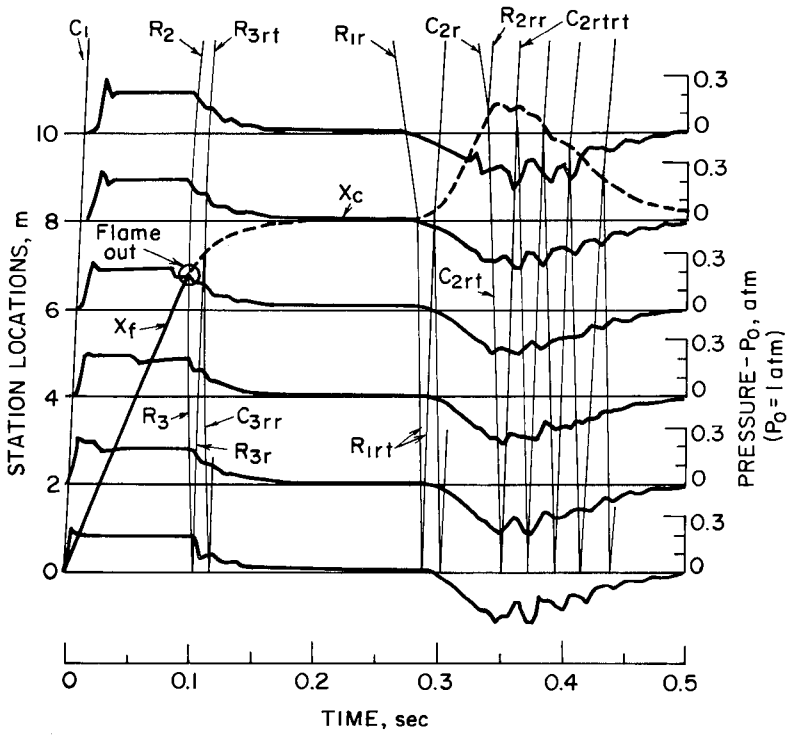

FIGURE 2. - The pressure histories at 0-, 2-, 4-, 6-, 8-, and 10-m stations from the closed end (ignition end).

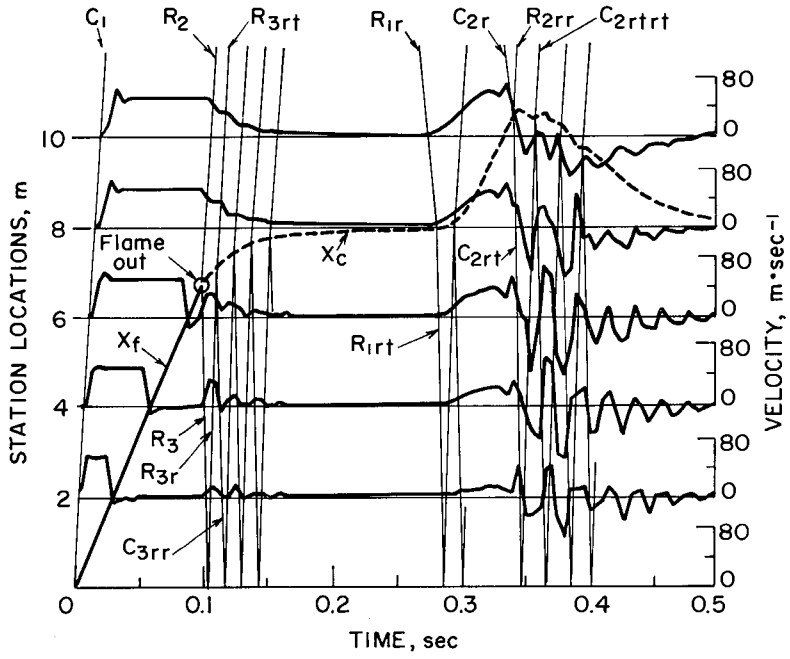

FIGURE 3. - Velocity histories at 0-, 2-, 4-, 6-, 8-, and 10-m stations from the closed end (ignition end).

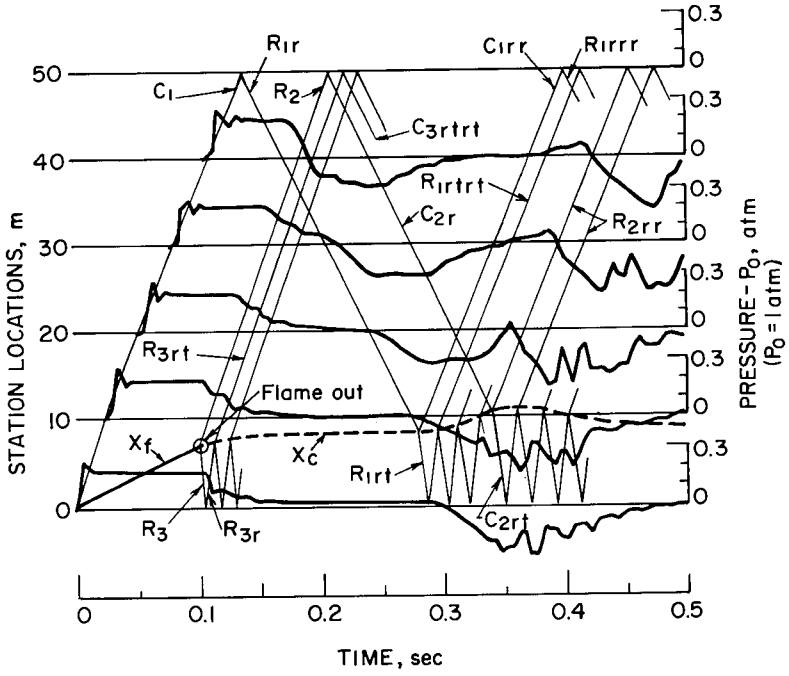

FIGURE 4. - Pressure histories at 0-, 10-, 20-, 30-, 40-, and 50-m stations from the closed end.

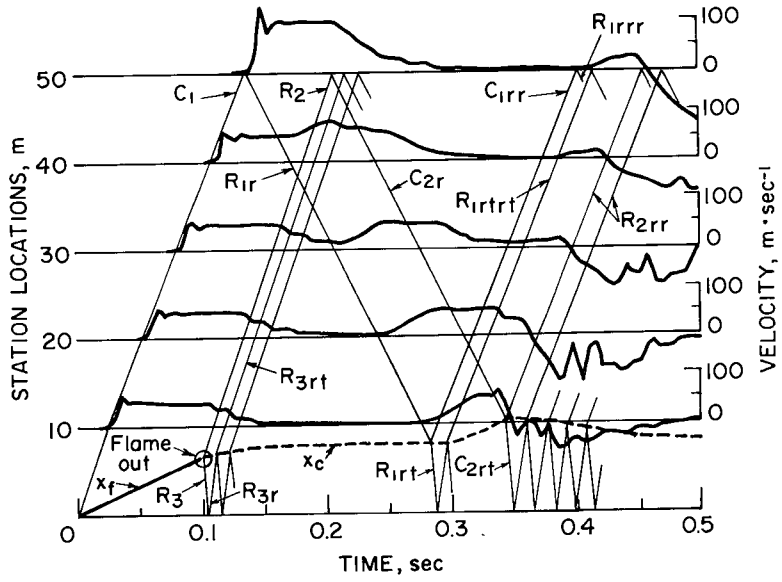

FIGURE 5. - Velocity histories at 0-, 10-, 20-, 30-, 40-, and 50-m stations from the closed end.

similar pressure and velocity histories at locations 0, 10, 20, 30, 40, and 50 m from the ignition. In both of these figures, the flame trajectory is indicated by a solid curve. The dashed line shows the trajectory of the contact surface. From the figures, it can be seen that the flame extinguishes after traveling a distance of 6.7 m.

Also shown in these figures are Mach lines corresponding to the leading edge of the more interesting features of the aerodynamic history. The nomenclature adopted distinguishes between compression (C) and rarefactions (R) and the subscripts identify the previous history of any particular wave. For example, the C_{1rtr} identifies a compression (C) that had its origin in the parent wave number 1 which intersects a boundary (open-end, closed-end, flame front, etc.) generating a reflected wave W_{1r} (W standing for either C or R depending on the nature of the boundary); this wave (W_{1r}) subsequently intersects another boundary generating a transmitted wave W_{1rt} and this transmitted wave in turn is reflected off another boundary, creating C_{1rtr}; the wave subscripts identify the ancestral types (reflected or transmitted) of each wave. In general, the greater the number of subscripts the weaker is the wave; with each boundary intersection the resultant waves are weakened.

In general, following ignition, the fireball grows as a hemispherical volume at the closed-end wall until it completely fills the cross section of the gallery. During this phase, as discussed in reference 13, the particle velocity upstream of the flame increases as t^2 until the flame front reaches the gallery sidewall. After the flame fills the cross section it propagates down the gallery. In this study the hemispherical growth process is ignored and it is assumed that following ignition the flame front is flat, completely filling the cross section of the gallery and propagating down the gallery unchanged in shape.

During flame propagation the expanding flame front pushes back the unburned gas ahead of it creating the pressure wave C_1 shown in the illustrations. The "overshoot" of pressure and velocity shown at the leading edge of C_1 in these illustrations is an inherent characteristic of the Lax-Wendroff algorithm, although it looks very similar to those associated with the hemispherical flame growth process. The pressure of the plateau ahead of the flame front in figure 2 has a value of 1.22 atm corresponding to a pressure increase of 0.22 atm (3.23 psig). Figure 3 shows that this pressure increase corresponds to a particle velocity of 56.6 m sec^{-1}. This overpressure compares favorably with the value of 2.94 psig calculated from the acoustic approximation given by the relation $\Delta P = u \cdot c_o \cdot \rho_o$, a difference of 9 percent. The pressure and particle velocity behind the flame front are not related through the acoustic relation; however, these values compare favorably with the measured pressure of 1.21 atm and an unburned gas velocity of 57.4 m sec^{-1}. Both calculated values differ from the experimental values by only 2 percent.

From figure 2 we see that as the flame front passes each station the velocity drops $(\chi-1)Su$ m sec^{-1}, and in this case, the gas velocity falls below zero momentarily, indicating a slight velocity reversal behind the flame front. Such a velocity reversal has often been observed in gallery experiments. To our knowledge the small pressure change across the flame front has been

clearly observed in only a few experiments, because the flame front in galleries is not sufficiently flat. Between the flame front and C_1 the pressure is constant at about 3 psig while the velocity remains zero. This is as expected for a nonaccelerating flame.

When the flame extinguishes after 0.1 sec at 6.7 m, two rarefactions are created, one propagating toward the closed end R_3, and one toward the open end R_2. Since the speed of sound in the hot-product gases is about 850 m sec^{-1}, it takes about 7 msec for R_3 to reach the closed end where it reflects as R_{3r}. R_{3r} travels back to the contact surface where the interaction of R_{3r} and the contact surface density discontinuity results in a transmitted rarefaction R_{3rt} and a reflected condensation C_{3rr}. Observe that an incident wave traveling in a high-density (unburned gas) medium that intersects a boundary to a lower-density medium (burned gas) reflects a wave of the same character as the incident wave. The transmitted wave is always of the same character as the incident wave regardless of the nature of the discontinuity. The disturbance within the burned zone continues to reflect between the closed end and the contact surface, producing a decaying resonance within the product cavity with a frequency of about 14 Hz ($\lambda \approx 60$ m). Every intersection of the wave reflected from the closed end with the contact surface produces a transmitted wave that travels toward the open end. The cavity resonance is evident in the oscillating pressure and velocity records seen in the region of these waves. This resonance decays rapidly because on each interaction with the contact surface it loses part of its energy to the train of transmitted waves, R_{3rt}, C_{3rrrt}, etc.

This resonance continues until the pressure in the burned zone is returned to ambient and the velocity to zero. At the same time the contact surface velocity slows to zero as the length of the burned zero expands to 8 m.

Meanwhile, the compression, C_1, has been traveling toward the open end at local sound speed in the unburned mixture (330 m sec^{-1}). Upon reaching the open end it reflects and returns back down the gallery as a rarefaction R_{1r}. Note that the velocity doubles at the open end as expected from conservation of momentum. R_{1r} passes through the oncoming rarefaction train R_2, R_{3rt}, etc., created by the burn-out and eventually at t = 0.27 sec reaches the contact surface. As before, the interaction of R_{1r} with the contact surface results in a transmitted R_{1rt} and reflected C_{1rr} wave. This interaction of R_{1r} and the contact surface results in a pronounced acceleration of the contact surface toward the open end. Because R_{1r} has a large wavelength (60 m) compared with the length of the burned gas zone (8 m), a pronounced resonance within the cavity is not observed. However, at 0.35 sec the shorter wavelength (8 m) disturbances (C_{2r}, C_{3rtr}, etc.) created by the flameout and subsequent burned gas cavity resonance returns to the contact surface creating both reflected (R_{2rr}, C_{3rtrr}, etc.) and transmitted (C_{2rt}, C_{3rtrt}, etc.) waves. Because the wavelenth of the transmitted waves are now comparable to the cavity length, a resonance is established corresponding to a frequency of about 5 Hz. This can be seen best in figure 3 where the oscillation in velocity are most pronounced. It is quite apparent from figure 3 that the amplitude of these oscillations is considerably larger by a factor of about 3 than

that created following flameout. We are apparently observing an amplification process associated with cavity resonance. We also notice that the contact surface moves from the 8-m station to about the 11-m station at which time C_{2r} contacts it and it begins a gradual (oscillatory) return to zero. Again, the oscillations decay rapidly and the pressure eventually returns to ambient, the velocity to zero, and the contact surface returns to 8 m. The calculations were stopped at 0.5 sec just before the R_{1rrr} returned from the open end.

The presence of the viscous term in the equations used had little effect on the history of the waves. There occurred a small decrease in the peak pressures as the waves moved through the gallery, but this is not noticeable in the plots. However, there is reason to believe that the value for the friction coefficient is not accurate. This requires further study.

Figure 6 shows the histories for the flame and contact surface, flame speed, particle velocity, gas density, and overpressure, all in the unburned gas immediately ahead of the flame (contact surface). Correspondingly, figure 7 shows the same information on the burned side of the flame (contact surface).

Comparing the particle velocity and overpressure traces in figure 6 we see that up to the time ($\sim$0.3 sec) of the interaction of the rarefaction wave, R_{1r}, and the contact surface, the unburned particle velocity, and overpressure are in phase and related to one another through the acoustic approximation $\Delta p = \rho_o c_o u$. After R_{1r} but before the interaction of the contact surface and the C_{2r} and C_{3r} waves created in flameout, the overpressure and particle velocity are 180° out of phase, but still related through the acoustic law. However, after the return of the C_{2r} and C_{3r} waves the overpressure and particle velocity no longer exhibit a fixed-phase relationship and the acoustic laws break down.

Interaction With a Flame Front (Phase 2)

In the second part of this study the situation where the flame is permitted to burn sufficiently long (0.8 sec) to observe the interaction of the flame front and the waves reflected off the open end was considered. The burning velocity in this study is taken to be 4.9 m sec^{-1}. Recall that although the burning velocity is constant the mass flux through the flame front is not constant. The mass flux through the flame is Su ρ_u where ρ_u is evaluated at the flame front. It is primarily through this variable (that is, mass flux) that the flame and aerodynamics are coupled in this study. Subsequent studies will be concerned with changes in flame shape and therefore aerodynamic effects on Su proper. We now determine if there is any significant difference between the interaction of the aerodynamics with a flame and a contact surface. Figures 8 through 11 show histories for the pressure and particle velocity at various stations along the gallery. The experiment was run twice as long as the previous study in order to see more reflections at the flame front.

The first major difference between this study and the preceding one is that in the absence of flameout there is only a parent wave, namely, C_1; all

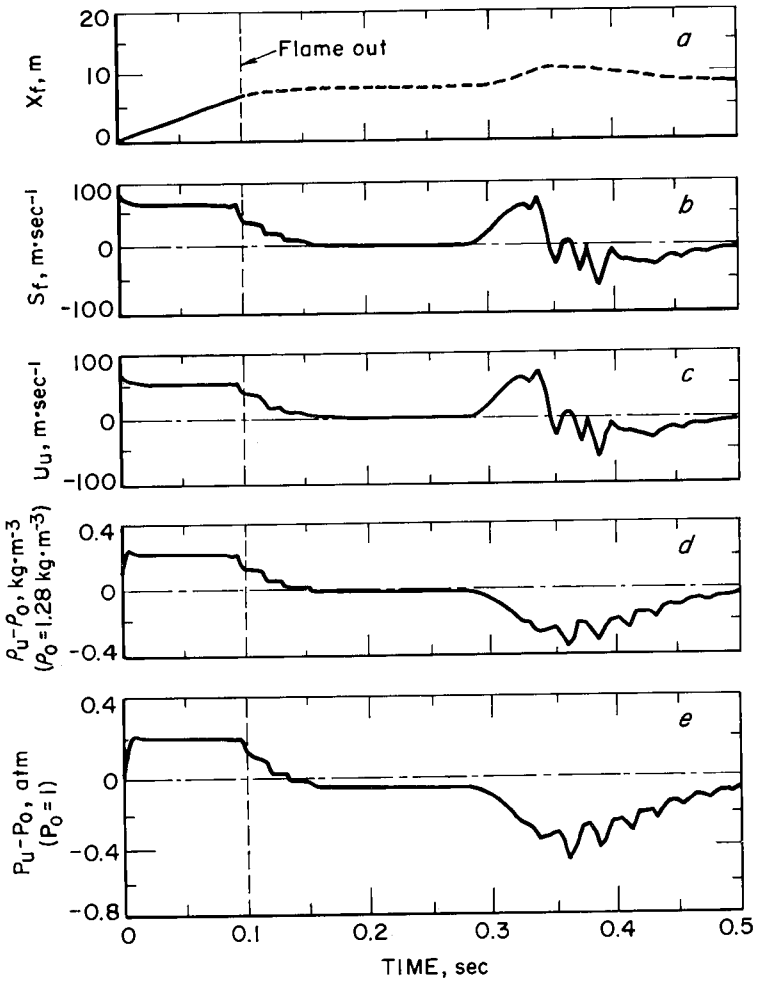

FIGURE 6. - Time histories of flame trajectory, x_f *(a)*; flame speed, S_f *(b)*; particle velocity *(c)*; density *(d)*; and pressure *(e)* at the unburned side of the flame front.

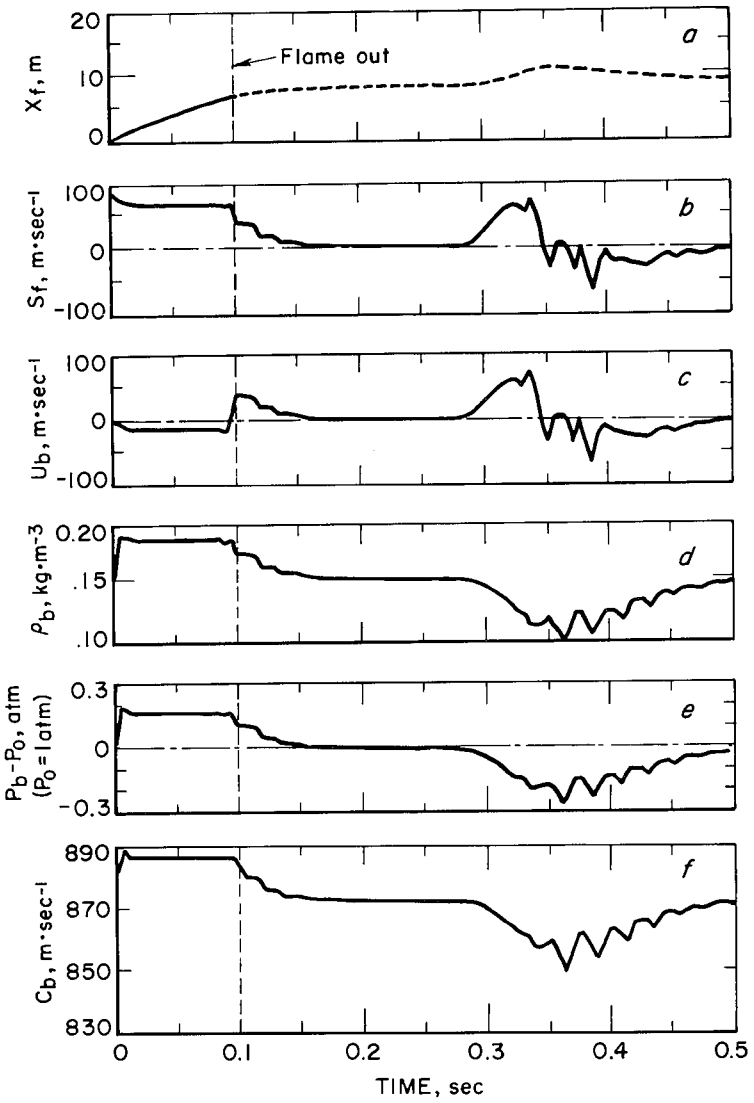

FIGURE 7. - Time histories of flame trajectory *(a)*; flame speed *(b)*; particle velocity *(c)*; density *(d)*; pressure *(e)*; and local sound speed *(f)* on the burned side of flame front.

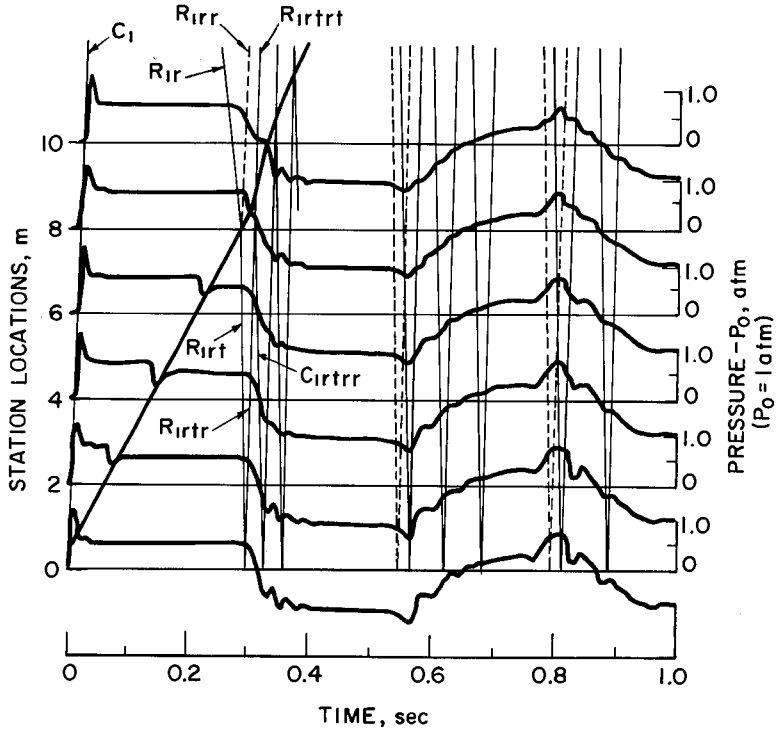

FIGURE 8. - Pressure histories at 0-, 2-, 4-, 6-, 8-, and 10-m stations from the closed end.

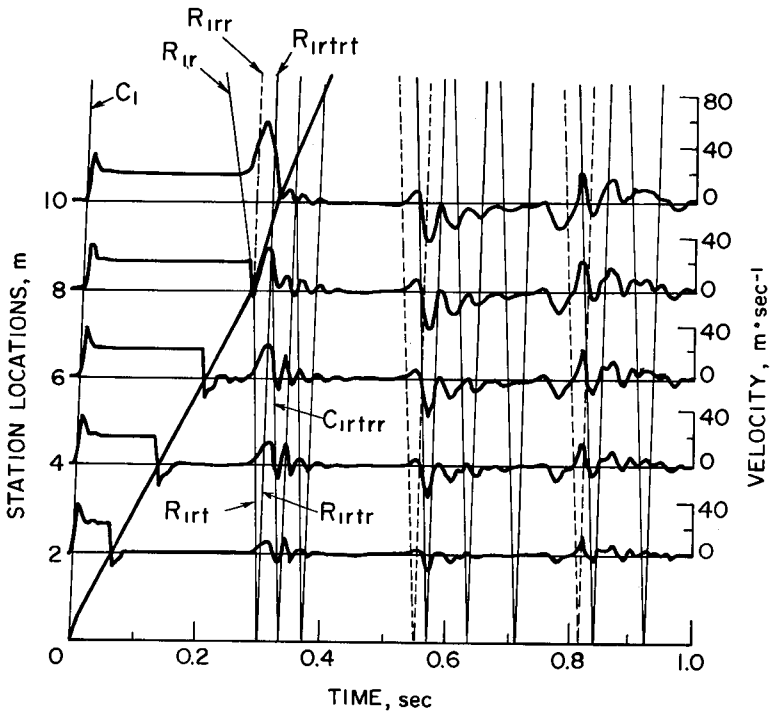

FIGURE 9. - Velocity histories at 0-, 2-, 4-, 6-, 8-, and 10-m stations from the closed end (ignition end).

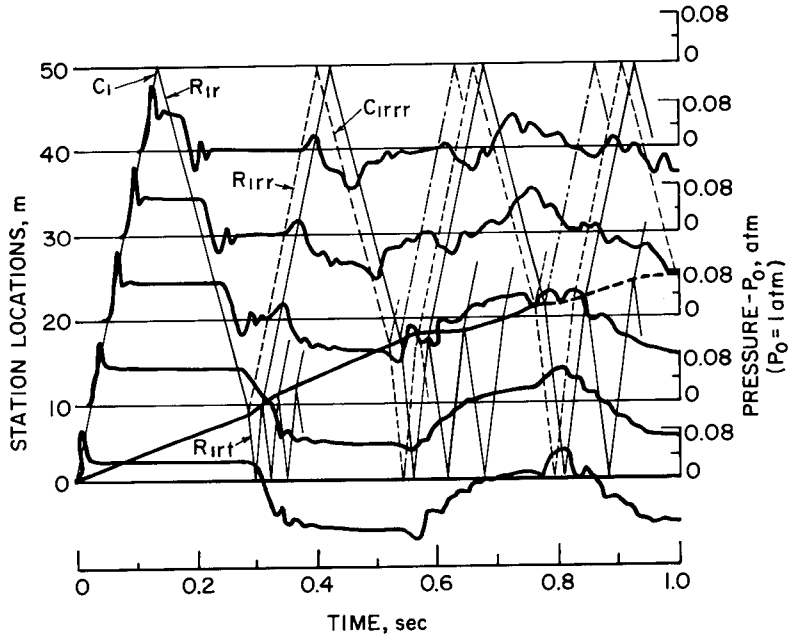

FIGURE 10. - Pressure histories at 0-, 10-, 20-, 30-, 40-, and 50-m stations from the closed end (ignition end). Flame is extinguished at 0.8 sec.

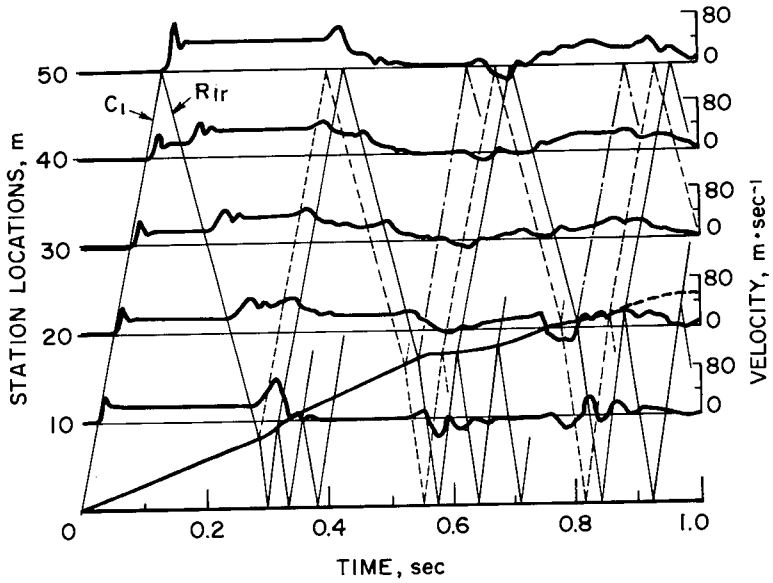

FIGURE 11. - Velocity histories at 0-, 10-, 20-, 30-, 40-, and 50-m stations from the closed end (ignition end). Flame extinguishes at 0.8 sec.

subsequent waves are decendents of C_1. The pressure of the plateau following the Lax-Wendroff spike amounts to 1.067 atm or 1.32 psig and the corresponding particle velocity is 21.9 m sec^{-1}. Again, the acoustic approximation for ΔP gives a value of 1.40 psig for this velocity, a difference of 6 pct. Figures 8 and 9 show the same pressure drop and velocity reversal across the flame front as was seen in the phase 1 experiment. Figure 10 shows C_1 reflect off the open end and return toward the flame as R_{1r} intersecting the flame at 0.28 sec, 8 m from the closed end. Following the intersection, the flame front is momentarily accelerated (although Su remains constant) toward the open end, but quickly returns to a constant flame speed after the burned gas cavity resonance decays. Figure 8 shows that, in the absence of flameout, the pressure never returns to a constant ambient state as it did in the previous case after flameout, although the particle velocity returns to zero following passage of the flame front and after decay of the burned cavity resonance.

With the return of the compression C_{1rrr} from the open end, the flame front decelerates and thereafter appears to exhibit a slow oscillatory motion. This mechanism explains the often observed (47) flame oscillations in galleries. At 0.55 sec the flame velocity goes to zero and the flame momentarily stops for a period of about 0.05 sec. Such phenomena have also been observed in gallery experiments.

The oscillatory behavior of the particle velocity in the resonance decaying region is not significantly different during the three periods, 0.3 to 0.4, 0.55 to 0.7, and 0.75 to 0.95 sec. There does not appear to be any aerodynamic amplification previously noticed in the flameout case.

Because of the relatively low overpressures in both cases (3 psig for the first and 1 psig for the second) and the relatively short gallery length (50 m), the initial disturbance never developes into a shock front.

Although the flame goes out at 0.8 sec and 22 m, except for a slight abrupt drop in the pressure and a corresponding increase in the particle velocity, the remaining aerodynamic features of the history are determined by the contact surface (indicated by the dotted lines in the illustrations) as well as the reflection and transmission of waves from the various surfaces.

Figures 12 and 13 show the density, pressure, and particle velocity histories adjacent to the flame on the unburned and burned sides of the flame front. Figure 12 shows that the particle velocity on the burned side of the flame remains negative at about 10 m sec^{-1} for the majority of the combustion history, only going positive when R_{1r} intersects the flame front at 0.3 sec and following flameout at 0.8 sec. Similarly, the particle velocity on the unburned side (fig. 12) remains positive except at 0.59 sec, where flame reversal occurs and the particle velocity momentarily goes negative. Since $S_f = u_u - Su$ and $Su = 4.9$ m sec^{-1}, whenever $u_u < 4.9$ m sec^{-1} $S_f < 0$, that is, flame reversal occurs.

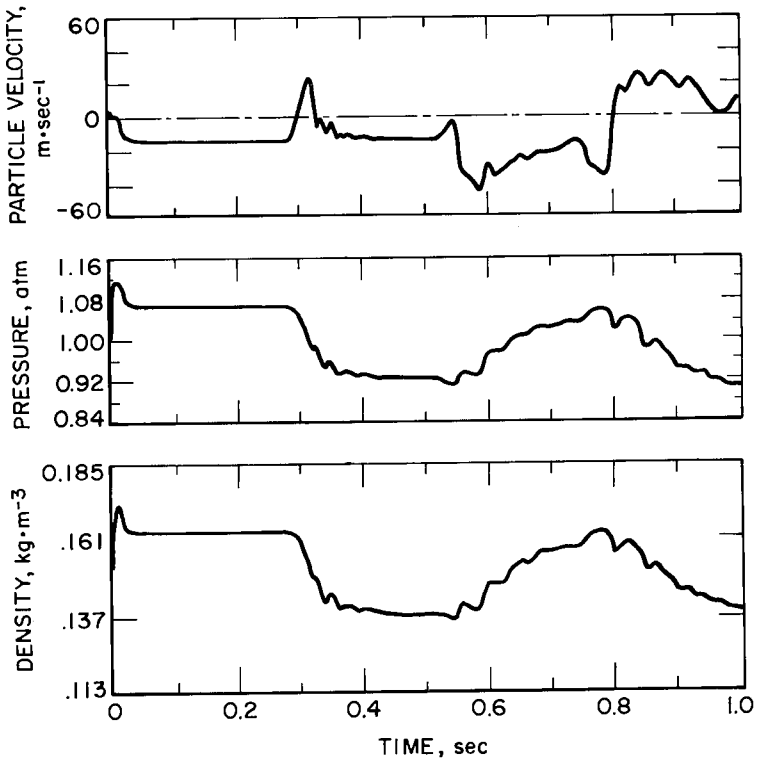

FIGURE 12. - Time histories of the variables at the burned side of the flame front.

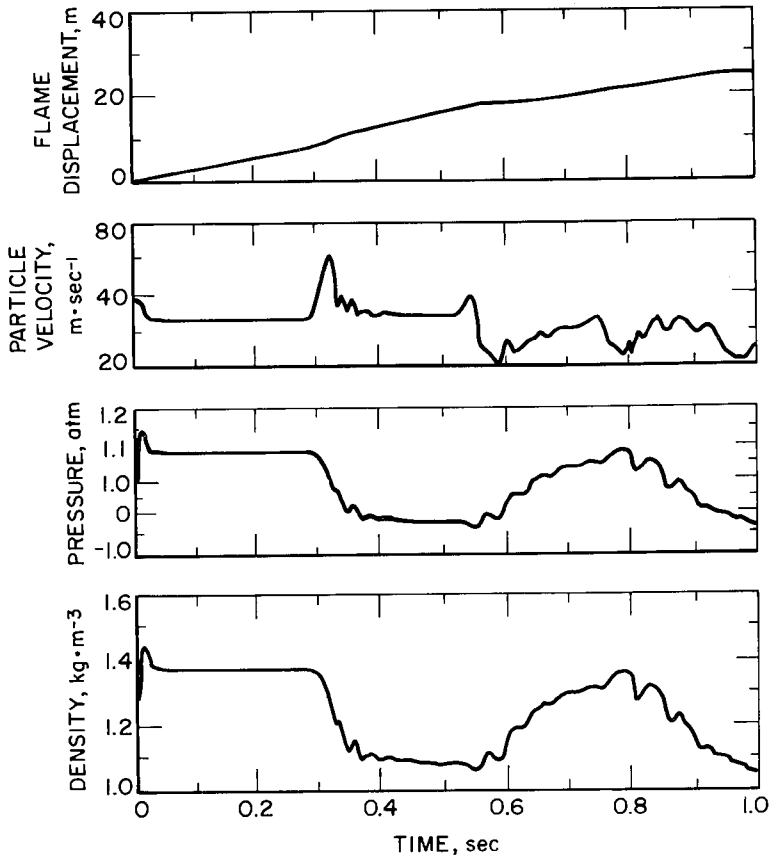

FIGURE 13. - Time histories of the variables at the unburned side of the flame front.

SUMMARY AND CONCLUSIONS

The conservation of mass, momentum, and energy equations for one-dimensional compressible unsteady flow in the conservation-law form have been solved for a deflagration propagating in a finite-length gallery. For this particular investigation the burning velocity Su remained fixed although the remaining system parameters (E, γ_u, γ_b, etc.) assumed functional values corresponding to a stoichiometric methane/air mixture. However, because of the relatively small changes in the pressure ($\leq \pm 5$ psig) the change in these parameters is insignificant.

In the first phase of the study the aerodynamic disturbance that developed ahead of the advancing flame traveled down the gallery at the speed of sound in the unburned gas and developed an overpressure of 3.23 psig and a particle velocity of 56.0 m sec^{-1} for a burning velocity of 7.4 m sec^{-1} and an expansion ratio of 8.5. The relationship between the pressure differential and velocity is satisfactorily described by the acoustic expression $\Delta P = u\, c_o\, \rho_o$. It was also observed that the act of sudden flame extinguishment generates strong rarefaction waves that travel away from the point of flameout in both directions. The interaction of the contact surface (after flameout) and the returning flameout rarefaction waves induce a resonance within the burned gas volume that decays rapidly to a quiescent state. Not unreasonably, the magnitude of the resonance depends on the relationship between the wavelength of the returning wave and the length of the burned gas cavity.

Note that as long as the burning velocity is constant, the slope of the flame trajectory is constant. The slope changes, however, whenever it interacts with the reflected waves from the boundaries and, in general, whenever it accelerates.

The presence of a viscous term in our equations had an insignificant affect on the aerodynamic history.

Unlike Jones (26), results in which a strong reverse flow of gas behind the flame front for an accelerating flame was found, only a momentary reverse flow immediately behind the flame front followed by an extended zero velocity region back to the ignition face was determined in this study.

In the second phase of this study where the flame was allowed to propagate until extinguished after interaction with the returning wave reflected from the open end of the gallery, flame front oscillation was observed. Although a burned gas cavity resonance is observed similar to that of the phase 1 case, there does not appear to be any appreciable pressure amplification.

FUTURE WORK

It is apparent from these investigations that the propagation characteristics of dust or gas flames in galleries are modified significantly by flame-induced aerodynamics. The implications of this fact, in view of the complex nature of coal-mine networks are far reaching, in that the history of flame

propagation in a coal mine network is not only a function of the combustion characteristics of the process, but also a function of the network geometry. In other words, effects such as changes in the cross sectional area, wall roughness, junctions, distance between junctions, etc., all have a pronounced effect on the history of a propagating flame. All of these factors can be studied within the present program and these results will be forthcoming in subsequent reports.

In addition to the above, an effort is currently underway to include source terms in the three conservation equations so as to provide for studying the effects of such processes as thermal losses to the walls, water-barrier spills, combustion inhibitor jets, dust entrainment, and ventilation flow on the system history. Since this inclusion does not appear to constitute a major modification to the existing program, the results of these studies should be forthcoming.

BIBLIOGRAPHY

1. Adams, G. K., and D. C. Pack. Some Observations on the Problem Between Deflagration and Detonation. 7th Internat. Symp. on Combustion at London and Oxford, England, Aug. 28-Sept. 3, 1958, Butterworths Scientific Publishers (London), 1959, pp. 812-819.

2. Akita, K. Flame Propagation in Combustible Fuel-Air Mixtures: Basic Thoery. Internat. Chem. Eng., v 11, No. 4, 1971, pp. 739-751.

3 Andrews, G. E., and D. Bradley. Determination of Burning Velocities: A Critical Review. Combustion and Flame, v. 18, 1972, pp. 133-153.

4. _____. The Burning Velocity of Methane-Air Mixtures. Combustion and Flame, v. 19, 1972, pp. 275-288.

5. Artingstall, G. On the Relation Between Flame and Blast in Coal-Dust Explosion. SMRE Res. Rept. 204, September 1961, 35 pp.

6. Artingstall, G., and T. C. Corlett. The Effect of Pressure Waves on the Propagation of Dust Explosions. Safety in Mines Res. Establishment (England) Res. Rept. 238, December 1965, 17 pp.

7. Bhaduri, D. Mechanism of Flame Propagation. J. Sci. and Ind. Res., v. 23, December 1964, pp. 502-506.

8. Bhaduri, D., C. B. Baxi, and B. S. Gill. Theoretical Evaluation of the Normal Velocity of Flame Propagation. Indian J. Technol., v. 6, August 1968, pp. 247-248.

9. Bhaduri, D., and S. Bandyopadhyay. Combustion in Coal-Dust Flame. Combustion and Flame, v. 17, 1971, pp. 15-24.

10. Beer, J. M., and N. A. Chigier. Combustion Aerodynamics. John Wiley & Sons, Inc., New York, 1972, 264 pp.

11. Bellman, R. Differential Quadrature: A Method for the Rapid Solution of Nonlinear Partial Differential Equations. J. Computational Phys., v. 10, No. 1, August 1972, pp. 40-52.

12. Bradley, D., and G. F. Hundy. Burning Velocity of Methane-Air Mixtures Using Hot Wire Anemometer in Closed Vessel Explosions. 13th Internat. Symp. on Combustion, University of Utah, Salt Lake City, Utah, Aug. 23-29, 1970, pp. 575-583. The Combustion Institute, Pittsburgh, Pa., 1190 pp.

13. Chi, D. N., and H. E. Perlee. Unsteady Unidimensional Flame Propagation in Coal Mine Passageways. Pres. at Soc. of Ind. and Appl. Mathematics Fall Meeting, Austin, Tex., Oct. 16-18, 1972, 14 pp.; available for consultation at Bureau of Mines, Pittsburgh Mining and Safety Research Center, Pittsburgh, Pa.

14. Courant, R., and K. O. Friedrichs. Supersonic Flow and Shock Waves. Interscience Publishers, Inc., New York, 1948, pp. 40-48.

15. Courant, R., K. Friedrichs, and H. Lewy. On the Partial Difference Equations of Mathematical Physics. IBM J., v. 2, 1967, pp. 215-234.

16. Cybulski, W. B. Correlation Between the Flame Velocity and the Dynamic Pressure Under the Conditions of Very Weak Coal-Dust Explosions. Bulletin De L'Academi Polonaise Des Sciences, v. 28, No. 12, 1970, pp. 9-17.

17. Doro Chemical Company, Thermal Research Laboratory. JANAF Thermochemical Tables. SN 03030872, Government Printing Office, Washington, D.C., 1970, unpaged.

18. Ferri, A. (ed.). Fundamental Data Obtained From Shock-Tube Experiments. Pergamon Press, New York, 1961, 415 pp.

19. Gordon, S., and B. J. McBride. Computer Program for Calculation of Complex Chemical Equilibrium Compositions, Rocket Performance, Incident, and Reflected Shocks, and Chapman-Jouguet Detonations. NASA Spec. Pub. 273, 1971, 245 pp.

20. Gunther, R., and G. Janisch. Measurement of Burning Velocity in a Flat Flame Front. Combustion and Flame, v. 19, 1972, pp 49-53.

21. Henkel, M. J., H. Hummel, and W. P. Spaulding. Theory of Flame Propagation of Flames. Part III: Numerical Integrations, 3d Symp. on Combustion, Flame, and Explosion Pehomena, Williams and Wilkins Co., Baltimore, Md., 1949, pp. 135-140.

22. Henkel, M. J., W. P. Spaulding, and J. O. Hirschfelder. Theory of Propagation of Flame. Part II: Approximate Solutions. 3d Symp. on Combustion, Flame, and Explosion Phenomena, Williams and Wilkins Co., Baltimore, Md., 1949, pp. 127-135.

23. Hirschfelder, J. O., and C. F. Curtiss. Theory of Propagation of Flames. Part II: General Equations, 3d Symp. on Combustion, Flame, and Explosion Phenomena, Williams and Wilkins Co., Baltimore, Md., 1949, pp. 121-127.

24. Issa, R. I., and D. B. Spalding. Unsteady One-Dimensional Compressible Frictional Flow With Heat Transfer. J. Mech. Eng. Sci., v 14, No. 6, 1972, pp. 365-369.

25. Istratov, A. G., and V. B. Librovich. On the Stability of Gasdynamic Discontinuities Associated With Chemical Reactions, The Case of Spherical Flame. Astronautica Acta, v. 14, 1969, pp. 453-467.

26. Jones, H. Accelerated Flames and Detonation in Gases. Proc. Royal Soc. (London), v. A248, 1958, pp. 333-349.

27. Karlovitz, B. The Growth and Burn-Out of Flame Surface in a Turbulent Stream. 7th Internat. Symp. on Combustion, London and Oxford, England, Aug. 28-Sept. 3, 1958, Butterworths Scientific Publishers (London), 1959, pp. 812-819.

28. Laderman, A. J., and A. K. Oppenheim. Initial Flame Acceleration in an Explosive Gas. Proc. Royal Soc. (London), v. A268, 1962, pp. 153-180.

29. Lax, P. D., and B. Wendroff. Systems of Conservation Laws. Communication on Pure and Appl. Mathematics, v. 13, 1960, pp. 217-237.

30. Lebecki, K. Research on the Theory of Dust Explosions. Safety in Mines Res. Establishment (England), Transl. No. 5489, 1967, 20 pp.

31. Liebman, I., and J. K. Richmond. Suppression of Coal Dust Explosion by Passive Barrier. Available for consultation at Bureau of Mines, Pittsburgh Mining and Safety Research Center, Pittsburgh, Pa.

32. Lister, M. M. The Numerical Solution of Hyperbolic Partial Differential Equations by the Method of Characteristics. In Mathematical Methods for Digital Computers, v. I, ed. by A. Ralston and H. Wilf, John Wiley & Sons, Inc., New York, 1967, pp. 165-179.

33. Markstein, G. H. Nonsteady Flame Propagation. The MacMillan Co., New York, 1964, pp. 5-14.

34. Mizutani, Y. Amplification of Turbulence Level by a Flame and Turbulent Flame Velocity. Combustion and Flame, v. 19, 1972, pp. 203-212.

35. Moretti, G. A Critical Analysis of Numerical Techniques: The Piston Driven Inviscid Flow. Polytech. Inst. of Brooklyn, Rept. 69-25, 1969, 43 pp.

36. Oppenheim, A. K. On the Dynamics of the Development of Detonation in Gaseous Medium. Archiwum Mechaniki Stosowanej, v. 2, No. 16, 1964, pp. 403-424; available from National Technical Information Service, Springfield, Va., AD622842.

37. Perlee, H. E., F. N. Fuller, and C. H. Saul. Constant Volume Flame Propagation. BuMines RI 7839, 1973, 44 pp.

38. Porter, R. W., and J. F. Coakley. Use of Characteristics for Boundaries in Time-Dependent Finite Difference Analysis of Multidimensional Gas Dynamics. Internat. J. for Numerical Methods in Engineering, v. 5, 1972, pp. 91-101.

39. Richmond, Kenneth J. Analysis of Blast Waves From Coal Dust Explosions. Pres. at the Conf. on Blast Waves Phenomena, Naval Weapons Station, Yorktown, Va., Nov. 13-15, 1973. Available for consultation at Pittsburgh Mining and Safety Research Center, Pittsburgh, Pa.

40. Richtmyer, R. D. Difference Methods for Initial Value Problems. Interscience Publishers, Inc., New York, 1964, 238 pp.

41. Roache, Patrick J. Computational Fluid Dynamics. Hermosa Publishers, Albuquerque, N. Mex., 1972, pp. 210-211.

42. Rubin, E. L., and S. Burstein. Difference Methods for the Inviscid and Viscous Equations of a Compressible Gas. J. Computational Phys., v. 2, No. 2, 1967, pp. 178-196.

43. Rudinger, G. Wave Diagrams for Unsteady Flow in Ducts. Van Nostrand Co., New York, 1955, 278 pp.

44. Salamandra, G. D. Interaction Between Flame and Shock Discontinuity. ARS J. Supplement, January 1960, pp. 73-75.

45. Shapiro, A. H. The Dynamics and Thermodynamics of Compressible Fluid Flow. V. 2, Ronald Press, New York, 1954, 1185 pp.

46. Shchelkin, K. I., and Ya. K. Troshin. Gasdynamics of Combustion. Mono Book Co., Baltimore, Md., 1965, 222 pp.

47. Singer, J. Dust Dispersals by Explosion-Induced Air Flow. Available for consulation at the Bureau of Mines Pittsburgh Mining and Safety Res Research Center, Pittsburgh, Pa.

48. Spalding, D. B. Some Thoughts on Flame Theory Combustion and Propulsions. 3d AGARD Colloquim, Pergamon Press, New York, 1958, pp. 269-306.

49. _____. Ends and Means in Flame Theory. 6th Symp. on Combustion, Yale Univ., New Haven, Conn., Aug. 19-24, 1956, Reinhold Publishing Co., New York, 1957, pp. 12-20.

50. _____. Approximate Solutions of Transient and Two-Dimensional Flame Propagation: Constant-Enthalpy Flames. Proc. Royal Soc. (London), v. A245, May-June 1958, pp. 352-372.

51. Spalding, D. B., P. L. Stephenson, and R. G. Taylor. A Calculation Procedure for the Prediction of Laminar Flame Speeds. Combustion and Flame, v. 17, 1971, pp. 55-64.

52. Summerfield, M., and H. Krier. Errors in Nonsteady Combustion Theory in the Past Decade (A Review). Am. Inst. Aeronautics and Astronautics 7th Aerospace Sciences Meeting, Paper No. 69-178, Jan. 20-22, 1969.

APPENDIX A.--TRANSFORMATION OF THE GOVERNING EQUATIONS INTO CONSERVATION-LAW FORM

The continuity equation 1 can be written as

$$\frac{\partial \rho}{\partial t} + u \frac{\partial \rho}{\partial x} + \rho \frac{\partial u}{\partial x} = 0$$

or

$$\frac{\partial \rho}{\partial t} + \frac{\partial}{\partial x} (\rho u) = 0 \ .$$

with the substitution $m = \rho \cdot u$, this becomes

$$\frac{\partial \rho}{\partial t} = - \frac{\partial m}{\partial x} \ . \tag{9}$$

Rewriting the equation of motion (2) as

$$\rho \frac{\partial u}{\partial t} = - \rho u \frac{\partial u}{\partial x} - \frac{\partial P}{\partial x} - \rho F$$

and adding $u \frac{\partial \rho}{\partial t}$ to both sides of this equation, one obtains

$$\rho \frac{\partial u}{\partial t} + u \frac{\partial \rho}{\partial t} = u \frac{\partial \rho}{\partial t} - \rho u \frac{\partial u}{\partial x} - \frac{\partial P}{\partial x} - \rho F \ .$$

Note that the left-hand side is $\frac{\partial m}{\partial t}$ while

$$u \frac{\partial \rho}{\partial t} = u \left[- \frac{\partial m}{\partial x} \right] ;$$

$$\frac{\partial m}{\partial t} = u \left[- \frac{\partial m}{\partial x} \right] - m \frac{\partial u}{\partial x} - \frac{\partial P}{\partial x} - \rho F$$

therefore,

$$= - \frac{\partial}{\partial x} \left[u \cdot m + P \right] - \rho \cdot F \ .$$

But

$$u = m/\rho \ .$$

Finally we obtain

$$\frac{\partial m}{\partial t} = - \frac{\partial}{\partial x} \left[m^2 / \rho + P \right] - \rho F \ . \tag{10}$$

With $e = c_v T$ and $(e + u^2/2) = \frac{1}{\rho}(\rho \cdot e + \rho u^2/2)$, equation 5 becomes

$$\frac{D}{Dt}\left[\frac{1}{\rho} E\right] = q - \frac{u}{\rho}\frac{\partial P}{\partial x} - \frac{P}{\rho}\frac{\partial u}{\partial x}$$

where $E = \rho \cdot e + \rho u^2/2$.

By the definition of substantive derivatives, we get

$$\frac{\partial}{\partial t}\left(\frac{1}{\rho} E\right) = - u \frac{\partial}{\partial x}\left(\frac{1}{\rho} E\right) - \frac{u}{\rho}\frac{\partial P}{\partial x} - \frac{P}{\rho}\frac{\partial u}{\partial x} + q$$

or

$$\frac{1}{\rho}\frac{\partial E}{\partial t} - \frac{E}{\rho^2}\frac{\partial \rho}{\partial t} = - u \frac{\partial}{\partial x}(E/\rho) - \frac{u}{\rho}\frac{\partial P}{\partial x} - \frac{P}{\rho}\frac{\partial u}{\partial x} + q \ .$$

$$\frac{\partial E}{\partial t} = \frac{E}{\rho}\frac{\partial \rho}{\partial t} - \rho \cdot u \frac{\partial}{\partial x}(E/\rho) - u\rho/\rho \frac{\partial P}{\partial x} - \rho \frac{P}{\rho}\frac{\partial u}{\partial x} + \rho q \ .$$

$$\frac{\partial E}{\partial t} = \frac{E}{\rho}\frac{\partial \rho}{\partial t} - m \frac{\partial}{\partial x}(E/\rho) - \frac{m}{\rho}\frac{\partial P}{\partial x} - \rho \frac{P}{\rho}\frac{\partial u}{\partial x} + \rho q \ .$$

Recall that $\partial\rho/\partial t = \partial m/\partial x$ then the above equation becomes

$$\frac{\partial E}{\partial t} = -\left\{\frac{E}{\rho}\frac{\partial m}{\partial x} + m \frac{\partial}{\partial x}(E/\rho)\right\} - \left\{\frac{m}{\rho}\frac{\partial P}{\partial x} + \rho \frac{P}{\rho}\frac{\partial u}{\partial x}\right\} + \rho q$$

$$= -\left\{\frac{\partial}{\partial x}[m \cdot E/\rho]\right\} - \left\{\frac{m}{\rho}\frac{\partial P}{\partial x} + P \frac{\partial}{\partial x}(m/\rho)\right\} + \rho q \ .$$

Hence

$$\frac{\partial E}{\partial t} = - \frac{\partial}{\partial x}[E \cdot m/\rho + m \cdot P/\rho] + \rho q \ .$$

Finally,

$$\frac{\partial E}{\partial t} = - \frac{\partial}{\partial x}\left[\frac{m}{\rho}(E + P)\right] + \rho q \ .$$

APPENDIX B.--EQUATIONS IN DIMENSIONLESS FORM

Two-Step-Lax-Wendroff Scheme

All the nondimensional variables are distinguished from the dimensional ones by a bar.

Thus, the expressions are written as follows:

$\bar{\rho} = \rho/\rho_o$,

$\bar{m} = m/m_o$ where $m_o = \rho_o C_o$ C_o = ambient sound speed,

$\bar{P} = P/P_o$,

$\bar{E} = E/P_o$,

$\bar{x} = x/LT$,

$\bar{C} = C/C_o$,

$\bar{t} = t/LT/C_o$, and finally,

$\bar{D} = D/LT$.

Substituting these expressions into the system of equations derived for "The Model" the following is obtained:

$$\frac{\partial \bar{\rho}}{\partial t} = - \frac{\partial \bar{m}}{\partial \bar{x}} \tag{B-1}$$

and

$$\frac{\partial \bar{m}}{\partial t} = - \frac{\partial}{\partial \bar{x}} \left[\frac{\bar{m}^2}{\bar{\rho}} + \frac{1}{\gamma_o} \bar{P} \right] - \frac{2f}{D} \cdot \frac{\bar{m}|\bar{m}|}{\bar{\rho}} \tag{B-2}$$

where

$$\gamma_o = \frac{C_o^2 \cdot P_o}{\rho_o} ,$$

and

$$\frac{\partial \bar{E}}{\partial t} = - \frac{\partial}{\partial x} \left[\frac{\bar{m}(\bar{E} + \bar{P})}{\rho} \right] + \bar{\rho} \cdot \bar{q} \ . \tag{B-3}$$

Note that only the equation of motion differs in its form from equation 10 by a factor $\frac{1}{\gamma_o}$ in the second term on the right-hand side.

Also,

$$\bar{P} = (\gamma - 1) \left(\bar{E} - \frac{1}{2} \gamma_o \frac{\bar{m}^2}{\bar{\rho}} \right) . \tag{B-4}$$

The boundary conditions remain the same in form. As for the initial conditions we have

$$\bar{u}(o,o) = 0,\ \bar{P}(o,o) = P_b/P_o,\ \bar{\rho}(o,o) = \rho_b/\rho_o,\ \bar{T}(o,o) = T_b/To$$

on the burned side and

$$\bar{u}(o,o) = Su/C_o,\ \bar{P}(o,o) = 1,\ \bar{\rho}(o,o) = 1,\ \bar{T}(o,o) = 1$$

on the unburned side. Elsewhere, all field variables are set to equal 1 except the gas velocity which is at zero.

The nondimensional forms for the conservation laws across the flame front are exactly the same as the dimensional ones.

By applying the same analysis, we obtain the following expression for the characteristic equations:

$$\frac{d\bar{u}}{dt} + \left(\frac{1}{\gamma_o}\right)\frac{1}{\bar{\rho}\,\bar{c}}\frac{d\bar{P}}{dt} = -\frac{2f}{\bar{D}}\bar{u}|\bar{u}|\left[1 - (\gamma-1)\frac{\bar{u}}{\bar{c}}\right] + (\gamma-1)\left(\frac{1}{\gamma_o}\right)\frac{\bar{q}}{\bar{c}}\ ; \tag{B-5}$$

$$\frac{d\bar{x}}{dt} = \bar{u} + \bar{c}\ ; \tag{B-6}$$

$$\frac{d\bar{u}}{dt} - \left(\frac{1}{\gamma_o}\right)\frac{1}{\bar{\rho}\,\bar{c}}\frac{d\bar{P}}{dt} = -\frac{2f}{\bar{D}}\left[1 + (\gamma-1)\frac{\bar{u}}{\bar{c}}\right] - (\gamma-1)\left(\frac{1}{\gamma_o}\right)\frac{\bar{q}}{\bar{c}}\ ; \tag{B-7}$$

$$\frac{d\bar{x}}{dt} = \bar{u} - \bar{c}\ ; \tag{B-8}$$

$$\frac{d\bar{P}}{dt} - (\gamma_o)\,\bar{c}^2\frac{d\bar{\rho}}{dt} = (\gamma_o)(\gamma-1)\frac{2f}{\bar{D}}\bar{\rho}\cdot\bar{u}|\bar{u}| + (\gamma-1)\,\bar{\rho}\cdot\bar{q}\ ; \tag{B-9}$$

and

$$\frac{d\bar{x}}{dt} = \bar{u}\ . \tag{B-10}$$

Note that again the only difference between the dimensional and nondimentional forms is the factor $\gamma_o = \dfrac{\rho_o c_o^2}{P_o}$.

In all subsequent discussions, we denote

$$FL(\bar{u},\bar{c}) = \frac{2f}{D}\,\bar{u}|\bar{u}|\left[1 - (\gamma-1)\,\frac{\bar{u}}{\bar{c}}\right] - (\gamma-1)\left(\frac{1}{\gamma_o}\right)\frac{\bar{q}}{\bar{c}}\,, \tag{B-11}$$

$$FR(\bar{u},\bar{c}) = \frac{2f}{D}\,\bar{u}|\bar{u}|\left[1 + (\gamma-1)\,\frac{\bar{u}}{\bar{c}}\right] + (\gamma-1)\left(\frac{1}{\gamma_o}\right)\frac{\bar{q}}{\bar{c}}\,, \tag{B-12}$$

and

$$G(\bar{\rho},\bar{u}) = (\gamma-1)\,\frac{2\cdot f}{D}\,\bar{\rho}\cdot\bar{u}|\bar{u}| + (\gamma-1)\,\bar{\rho}\cdot\bar{q}\,. \tag{B-13}$$

The bars will also be removed since the presence or absence of the factor γ_o will unambiguously determine whether an expression is in a nondimensional form.

APPENDIX C.--DISTINCT CASES RESULTING FROM THE POSITION OF THE FLAME FRONT RELATIVE TO A GIVEN MESH

The descriptive partial differential equations are solved on both sides of the flame front and the solutions are matched at the flame front through appropriate boundary conditions using the method of characteristics. In applying the boundary conditions at the flame front it is necessary to consider the totality of possible geometrical arrangements of the flame trajectory within the finite difference mesh. Figure C-1 illustrates the total arrangements considered for this problem. In each arrangement, distinct computational procedures are used.

The nodal points are denoted by $x_1, x_2, \ldots, x_{N+1}$. xF^n and xF^{n+1} are locations of flame front at time $t = n \cdot \Delta t$ and $t = (n+1)\Delta t$.

The first category (fig. C-1) refers to the situations where $x_1 \leq xF^n$ and/or $xF^{n+1} \leq x_3$; that is, either xF^{n+1} or xF^n may be greater than x_3 but less than x_4; the second category (fig. C-2) refers to the condition that $x_3 \leq xF^n$ and $xF^{n+1} \leq x_{N-1}$, while the last category is the case when $x_{N-1} > xF^{n+1}$ or $x_{N-1} > xF^n$. Dotted lines in figures C-1 and C-2 denotes flame trajectory.

Category III is the case where $x_{N-1} \leq xF^n$, $xF^{n+1} \leq x_{N+1}$, namely, in the vicinity of the open end. Since it is a mirror image of category I, detailed diagrams are omitted.

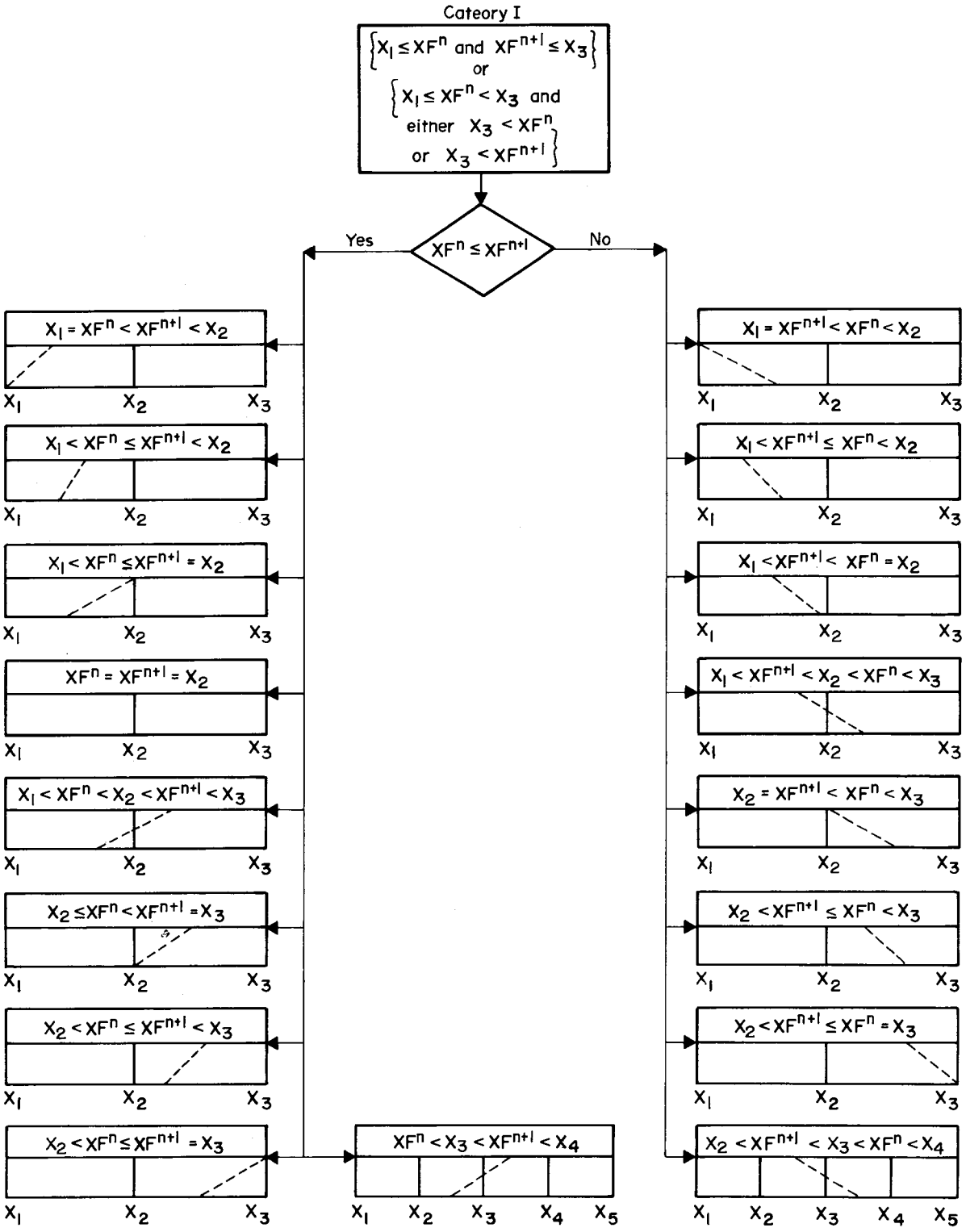

FIGURE C-1. - Category I.

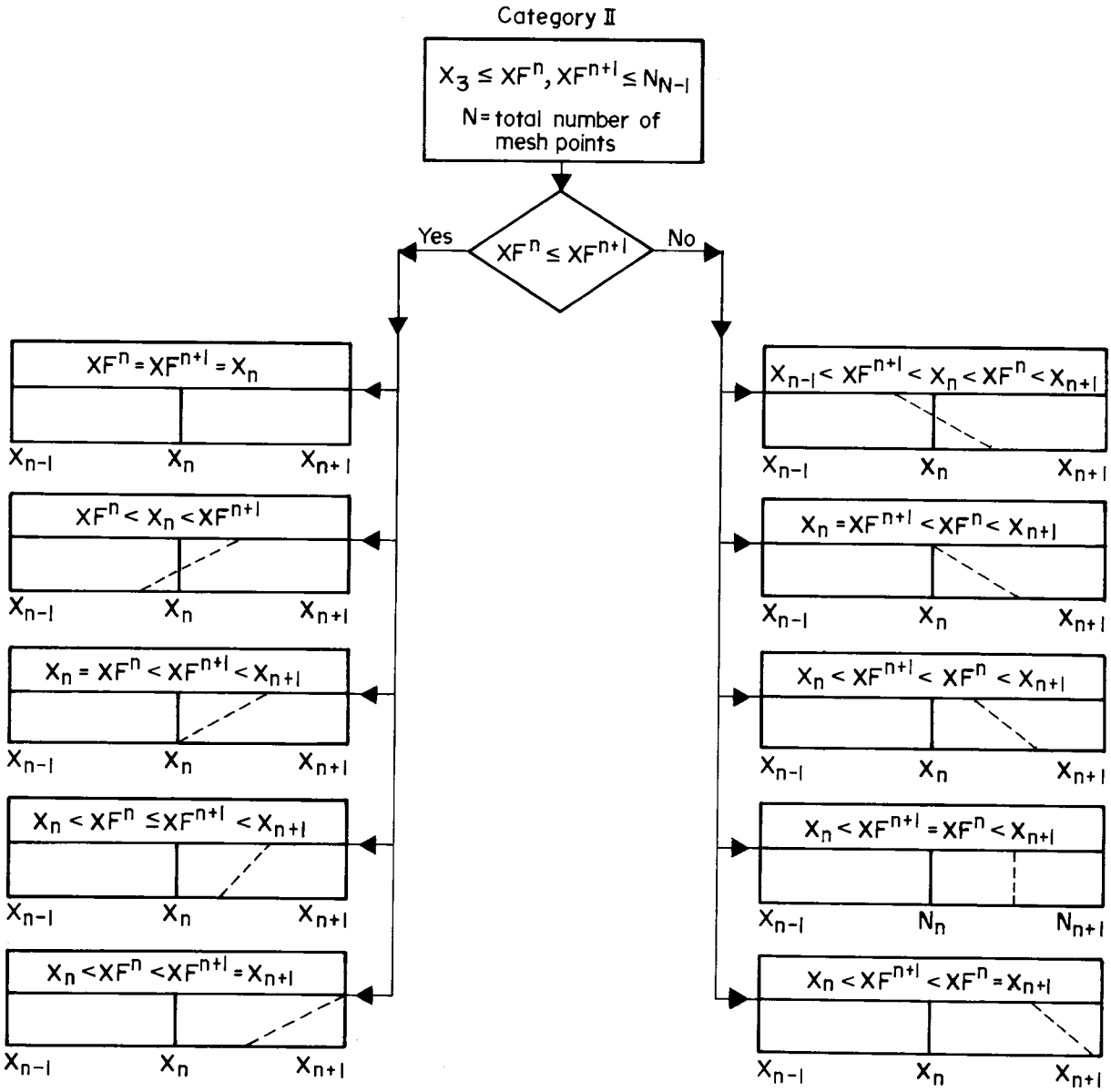

FIGURE C-2. - Category II.

APPENDIX D.--NUMERICAL ALGORITHMS

Applying the modified two-step-Lax-Wendroff scheme (35) to equations 9 through 11 in nondimensional form (appendix C), we obtain the following working equations (see fig. 1):

$$\rho_{n+\frac{1}{2}}^{t+\Delta t} = \frac{1}{2}\left(\rho_{n+1}^{t} + \rho_{n}^{t}\right) - \frac{\Delta t}{\Delta x}\left(m_{n+1}^{t} - m_{n}^{t}\right) . \tag{D-1}$$

$$\rho_{n}^{t+\Delta t} = \rho_{n}^{t} - \left(\frac{1}{4}\right)\left(\frac{\Delta t}{\Delta x}\right)\left[m_{n+1}^{t} - m_{n-1}^{t} + 2\left(m_{n+\frac{1}{2}}^{t+\Delta t} - m_{n-\frac{1}{2}}^{t+\Delta t}\right)\right] . \tag{D-2}$$

$$m_{n+\frac{1}{2}}^{t+\Delta t} = \frac{1}{2}\left(m_{n+1}^{t} + m_{n}^{t}\right) - \frac{\Delta t}{\Delta x}\left[\frac{\left(m_{n+1}^{t}\right)^{2}}{\rho_{n+1}^{t}} - \frac{\left(m_{n}^{t}\right)^{2}}{\rho_{n}^{t}} + \left(\frac{P_{n+1}^{t}}{\gamma_{o}} - \frac{P_{n}^{t}}{\gamma_{o}}\right)\right] .$$

$$- \frac{f}{D}\Delta t\left[\frac{m_{n+1}^{t}\left|m_{n+1}^{t}\right|}{\rho_{n+1}^{t}} + \frac{m_{n}^{t}\left|m_{n}^{t}\right|}{\rho_{n}^{t}}\right] . \tag{D-3}$$

$$m_{n}^{t+\Delta t} = m_{n}^{t} - \left(\frac{\Delta t}{\Delta x}\right)\left\{\frac{\left(m_{n+1}^{t}\right)^{2}}{\rho_{n+1}^{t}} - \frac{\left(m_{n-1}^{t}\right)^{2}}{\rho_{n-1}^{t}} + \frac{P_{n+1}}{\gamma_{o}} - \frac{P_{n-1}^{t}}{\gamma_{o}}\right.$$

$$\left. + 2\left[\frac{\left(m_{n+\frac{1}{2}}^{t+\Delta t}\right)^{2}}{\rho_{n+\frac{1}{2}}^{t+\Delta t}} - \frac{\left(m_{n-\frac{1}{2}}^{t+\Delta t}\right)^{2}}{\rho_{n-\frac{1}{2}}^{t+\Delta t}} + \frac{P_{n+\frac{1}{2}}^{t+\Delta t}}{\gamma_{o}} - \frac{P_{n-\frac{1}{2}}^{t+\Delta t}}{\gamma_{o}}\right]\right\}$$

$$- \frac{f}{D}\Delta t\left[\frac{m_{n+\frac{1}{2}}^{t+\Delta t}\left|m_{n+\frac{1}{2}}^{t+\Delta t}\right|}{\rho_{n+\frac{1}{2}}^{t+\Delta t}} + \frac{m_{n-\frac{1}{2}}^{t+\Delta t}\left|m_{n-\frac{1}{2}}^{t+\Delta t}\right|}{\rho_{n-\frac{1}{2}}^{t+\Delta t}}\right] . \tag{D-4}$$

$$E_{n+\frac{1}{2}}^{t+\Delta t} = \frac{1}{2}\left(E_{n+1}^{t} + E_{n}^{t}\right)$$

$$- \frac{\Delta t}{\Delta x}\left[\frac{m_{n+1}^{t}}{\rho_{n+1}^{t}}\left(E_{n+1}^{t} + P_{n+1}^{t}\right) - \frac{m_{n}^{t}}{\rho_{n}^{t}}\left(E_{n}^{t} + P_{n}^{t}\right)\right]$$

$$+ \Delta t\left[\rho_{n+1}^{t} q_{n+1}^{t} + \rho_{n}^{t} q_{n}^{t}\right]/2.00 . \tag{D-5}$$

$$E_n^{t+\Delta t} = E_n^t - \left(\frac{1}{4}\right)\left(\frac{\Delta t}{\Delta x}\right)\left\{\frac{m_{n+1}^t}{\rho_{n+1}^t}\left(E_{n+1}^t + P_{n+1}^t\right)\right.$$

$$- \frac{m_{n-1}^t}{\rho_{n-1}^t}\left(E_{n-1}^t + P_{n-1}^t\right) + 2\left[\frac{m_{n+\frac{1}{2}}^{t+\Delta t}}{\rho_{n+\frac{1}{2}}^{t+\Delta t}}\left(E_{n+\frac{1}{2}}^{t+\Delta t} + P_{n+\frac{1}{2}}^{t+\Delta t}\right)\right.$$

$$\left.\left. - \frac{m_{n-\frac{1}{2}}^{t+\Delta t}}{\rho_{n-\frac{1}{2}}^{t+\Delta t}}\left(E_{n-\frac{1}{2}}^{t+\Delta t} + P_{n-\frac{1}{2}}^{t+\Delta t}\right)\right\}\right.$$

$$+ \Delta t\left\{\rho_{n+\frac{1}{2}}^{t+\Delta t}\, q_{n+\frac{1}{2}}^{t+\Delta t} - \rho_{n-\frac{1}{2}}^{t+\Delta t}\, q_{n-\frac{1}{2}}^{t+\Delta t}\right\}. \qquad \text{(D-6)}$$

Note that $P_n^t = (\gamma-1)\left[E_n^t - \frac{\gamma_o}{2}\frac{(m_n^t)^2}{\rho_n^t}\right]$.

APPENDIX E.--NUMERICAL SCHEMES AT THE BOUNDARIES

In this appendix the finite difference expressions for the boundary conditions at the three boundaries (closed end, open end, and flame front) are derived. The mesh point labeled A, B, C, D, ZL, ZR, XF^t, and $XF^{t\,t\Delta t}$ refer to coordinate labels shown in figure 2.

Across Flame Front

See figure 2 for the definitions of the points denoted by A, B, C, D, ZR, XF^t, and $XF^{t+\Delta t}$. The last two are sometimes denoted as XF^n and XF^{n+1}. P_{ZL}, P_{ZR}, U_{ZL}, U_{ZR}, etc., are pressure and velocity at the points ZR, ZL, etc. The subscripts u and b refer to flow fields on the unburned and burned side, respectively.

The finite difference analogues (first order) of equations B-5 and B-6 are given as follows:

$$\frac{U_D - U_{ZL}}{\Delta t} + \left(\frac{1}{\gamma_o}\right)\frac{1}{\rho_{ZL}\,C_{ZL}}\frac{P_D - P_{ZL}}{\Delta t} = -\,FL\,(u_{ZL},\,C_{ZL});$$

and

$$\frac{\Delta t}{B - ZL} = \frac{1}{U_{ZL} + C_{ZL}}$$

where $U_d = U_b$ and $P_D = P_b$. Therefore, for the burned side we have

$$U_b = -\left(\frac{1}{\gamma_o}\right)\left(\frac{1}{\rho_{ZL}\,C_{ZL}}\right)P_b + \left(\frac{1}{\gamma_o}\right)\left(\frac{1}{\rho_{ZL}\,C_{ZL}}\right)P_{ZL} + U_{ZL} - \Delta t\;FL(U_{ZL},\,C_{ZL}), \tag{E-1}$$

and

$$B - ZL = \Delta t\,(U_{ZL} + C_{ZL})\,. \tag{E-2}$$

Similarly, on the unburned side equations B-8 and B-9 become

$$U_u = \left(\frac{1}{\gamma_o}\right)\left(\frac{1}{\rho_{ZR}\,C_{ZR}}\right)P_u - \left(\frac{1}{\gamma_o}\right)\left(\frac{1}{\rho_{ZR}\,C_{ZR}}\right)P_{ZR}$$

$$+ U_{ZR} - \Delta t\cdot FR\,(U_{ZR},\,C_{ZR}) \tag{E-3}$$

and

$$B - ZR = \Delta t\,(U_{ZR} - C_{ZR})\,, \tag{E-4}$$

while equations B-9 and B-10 are transformed into

$$P_u = (\gamma_o)(C_{xp}^2)\,\rho_u - (\gamma_o)\,\rho_{xp} + P_{xp} + (\gamma_o)\,\Delta t\;G(\rho_{xp},\,U_{xp}) \tag{E-5}$$

$$B - xp = U_{xp}\cdot\Delta t\,. \tag{E-6}$$

Solving these together with the boundary conditions equations 15 through 17 across the flame front we obtain the final expression

$$U_b^{t+\Delta t} = \Big\{ -\beta(\chi-1)Su + \left(\frac{1}{\gamma_o}\right)(P_{ZL}\cdot K - P_{ZR}) + (\alpha\cdot K\cdot U_{ZL} + \beta\, U_{ZR}) - \Delta t\,(\alpha\cdot K\cdot FL(U_{ZL}, C_{ZL}) + \beta\, FR(U_{ZR}, C_{ZR}))\Big\} / (\alpha+\beta)\ ,$$

where $\alpha = \rho_{ZL}\cdot C_{ZL}$,

$\beta = \rho_{ZR}\cdot C_{ZR}$,

and $K = 1 + \gamma_b\ \chi(\chi-1)\left(\frac{Su}{C_b}\right)^2$.

$$U_u^{t+\Delta t} = U_b^{t+\Delta t} + (\chi-1)\ Su\ , \tag{E-8}$$

$$P_b^{t+\Delta t} = -\gamma_o\alpha\ U_b^{t+\Delta t} + P_{ZL} + \gamma_o\alpha\ U_{ZL} - \Delta t\cdot\gamma_o\alpha\cdot FL(U_{ZL}, C_{ZL})\ . \tag{E-9}$$

$$P_u{}^{t+\Delta t} = K\ P_b^{t+\Delta t}\ , \tag{E-10}$$

$$\rho_u^{t+\Delta t} = \{(P_u^{t+\Delta t} - P_{xp})/\gamma_o + C_{xp}^2\ \rho_{xp} - \Delta t\cdot G(U_{xp}, \rho_{xp})\}/C_{xp}^2\ , \tag{E-11}$$

and

$$\rho_b^{t+\Delta t} = \rho_u^{t+\Delta t}/\chi\ . \tag{E-12}$$

$m_u^{t+\Delta t}$, $m_b^{t+\Delta t}$, $E_u^{t+\Delta t}$, and $E_b^{t+\Delta t}$ can be computed from the transformations. In the expressions above, we use the following:

$$U_{ZL} = \frac{(xF^t - xF^{t+\Delta t}) + (xF^{t+\Delta t} - A)\ U_b^t + \Delta t\ (U_A^t - U_b^t)\ C_{ZL}}{[(xF^t - A) + \Delta t\ (U_b^t - U_A^t)]}$$

and

$$ZL = xF^{t+\Delta t} - \Delta t\ (U_{ZL} + C_{ZL})\ , \tag{E-14}$$

where

$$C_{ZL} \approx \frac{1}{2}\ (C_A + C_b)\ .$$

Let

$$\lambda = \left(\frac{xF^t - ZL}{xF^t - A}\right);$$

then

$$\rho_{ZL} = \lambda\rho_A + (1-\lambda)\rho_b \tag{E-15}$$

and

$$P_{ZL} = \lambda P_A + (1-\lambda)P_b\ . \tag{E-16}$$

$$U_{ZR} = \frac{(C-xF^{t+\Delta t})\ U_u^t + (xF^{t+\Delta t}-xF^t)\ U_c^t + \Delta t\ (U_c^t-U_u^t)\cdot C_{ZR}}{[(C-xF^t) + \Delta t\ (U_c^t-U_u^t)]}\ , \tag{E-17}$$

with
$$ZR = xF^{t+\Delta t} - \Delta t\ (U_{ZR}-C_{ZR})\ , \tag{E-18}$$

where
$$C_{ZR} \simeq \frac{1}{2}\ (C_c^t + C_u^t)\ .$$

For
$$\delta = \frac{(C-ZR)}{(C-xF^t)}\ ,$$

$$\rho_{ZR} = \delta\cdot\rho_u^t + (1-\delta)\ \rho_c^t \tag{E-19}$$

and
$$P_{ZR} = \delta_u\cdot P_u^t + (1-\delta)\ P_c^t\ . \tag{E-20}$$

Finally,

$$U_{xp} = \frac{(ZR-xF^{t+\Delta t})\ U_u^t + (xF^{t+\Delta t}-xF^t)\cdot U_{ZR}^t}{[(ZR-xF^t) + \Delta t\ (U_{Z_R}^t-U_u^t)]} \tag{E-21}$$

in which
$$xP = xF^{t+\Delta t} - \Delta t\ U_{xp}\ , \tag{E-22}$$

$$\rho_{xp} = \Psi\cdot\rho_u^t + (1-\Psi)\ \rho_{ZR}\ , \tag{E-23}$$

and
$$P_{xp} = \Psi P_u^t + (1-\Psi)\ P_{ZR}$$

where
$$\Psi = \frac{ZR - xP}{ZR - xF^t}\ .$$

<u>At the Closed End</u>

When the flame is not at the vicinity of the closed end, x_1, the following expressions are used (fig. E-1):

$$U_1^{t+\Delta t} = 0 \tag{E-25}$$

$$P_1^{t+\Delta t} = P_{ZR} + (\gamma_o\cdot\rho_{ZR}\cdot C_{ZR})[-U_{ZR} + \Delta t\cdot FR(U_{ZR}, C_{ZR})] \tag{E-26}$$

and
$$\rho_1^{t+\Delta t} = \frac{1}{C_1^2}\left[\frac{1}{\gamma_o}\ (P_1^{t+\Delta t}-P_1^t) - \Delta t.G(\rho_1, C_1)\right] + \rho_1^t\ , \tag{E-27}$$

where
$$G(\rho_1, C_1) = \frac{(\gamma_b-1)}{\gamma_o}\cdot\rho_1^t\cdot q_1^t + (\gamma_b-1)\cdot\frac{2f}{D}\ \rho_1^t\cdot U_1^t\left|U_1^t\right|\ ,$$

$$FR\ (U_{ZR}, C_{ZR}) = \frac{(\gamma_b-1)}{\gamma_o}\cdot\frac{q_{ZR}}{C_{ZR}} + \frac{2\cdot f}{D}\ UZR\left|UZR\right|\cdot\left[1+(\gamma_b-1)\ \frac{UZR}{CZR}\right],$$

$$U_{ZR} = \frac{\Delta t}{\Delta x}\left(\frac{1}{1+\frac{\Delta t}{\Delta x}\cdot U_2^t}\right)\cdot U_2^t\cdot C_{ZR}\ ,$$

$$ZR = x_1 - \Delta t\ (U_{ZR} + C_{ZR})\ ,$$

$$\rho_{ZR} = \left(\frac{x_2 - ZR}{\Delta x}\right)\rho_1^t + \left(\frac{ZR - x_1}{\Delta x}\right)\rho_2^t\ ,$$

$$P_{ZR} = \left(\frac{x_2 - ZR}{\Delta x}\right)P_1^t + \left(\frac{ZR - x_1}{\Delta x}\right)P_2^t\ ,$$

$$U_{xp} = U_1^t = 0\ ,$$

$$\rho_{xp} = \rho_1^t\ ,\ P_{xp} = P_1^t\ ,\ \text{and}\ C_{xp} = C_1^t\ .$$

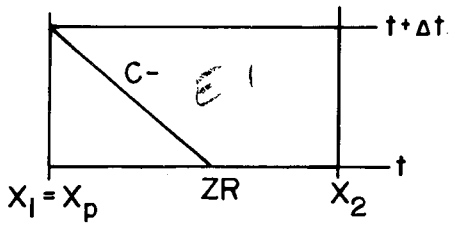

FIGURE E-1. - Boundary geometry at closed end.

At the Open End, x_{N+1}

In this case, we again assume that the flame front is at least at a distance of Δx from x_{N+1}, as seen in figure E-2.

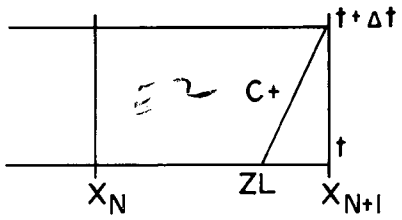

FIGURE E-2. - Boundary geometry at

Furthermore,
$$P_{N+1}^{t+\Delta t} = 1\ , \tag{E-28}$$

$$U_{N+1}^{t+\Delta t} = \left(\frac{1}{\gamma_o}\right)\left(\frac{1}{P_{ZL}\ C_{ZL}}\right)(P_{ZL} - P_{N+1}^{t+\Delta t})$$

$$+ U_{ZL} - \Delta t \cdot FL\ (U_{ZL}, C_{ZL})\ ,$$

and
$$\rho_{N+1}^{t+\Delta t} = \rho_{xp}^t + \frac{1}{C_{xp}^2}\left[\frac{P_{N+1}^{t+\Delta t} - P_{xp}^t}{\gamma_o} - \Delta t \cdot G(\rho_{xp}, U_{xp})\right]\ , \tag{E-29}$$

where $$FL = \frac{-(\gamma_u - 1)}{\gamma_o}\left(\frac{q_{ZL}}{C_{ZL}}\right) + \frac{2 \cdot f}{D} U_{ZL} \left|U_{ZL}\right| \cdot \left[1 - (\gamma_u - 1)\frac{U_{ZL}}{C_{ZL}}\right] ,$$

$$G = \frac{(\gamma_u - 1)}{\gamma_o} \cdot \rho_{N+1}^t \cdot q_{N+1}^t + (\gamma_u - 1) \cdot \frac{2f}{D} \cdot \rho_{N+1}^t \cdot U_{N+1}^t \left|U_{N+1}^t\right| ,$$

$$U_{ZL} = \frac{\Delta x \cdot U_{N+1}^t + \Delta t \ (U_N^t - U_{N+1}^t) \cdot C_{ZL}}{1 - \left(\frac{\Delta t}{\Delta x}\right)(U_N^t - U_{N+1}^t)} ,$$

$$ZL = x_{N+1} - \Delta t \cdot (U_{ZL} + C_{ZL}) ,$$

$$\rho_{ZL} = \left(\frac{x_{N+1} - ZL}{\Delta x}\right)\rho_N^t + \left(\frac{ZL - x_N}{\Delta x}\right)\rho_{N+1}^t ,$$

$$P_{ZL} = \left(\frac{x_{N+1} - ZL}{\Delta x}\right)P_N^t + \left(\frac{ZL - x_N}{\Delta x}\right)P_{N+1}^t ,$$

$$U_{xp} = U_{N+1}^t \Big/ \left[1 + \frac{\Delta t}{\Delta x}\ (U_{N+1}^t - U_N^t)\right] ,$$

$$xp = x_{N+1} - \Delta t \cdot U_{xp} ,$$

$$\rho_{xp} = (\rho_N^t)(x_{N+1} - xp)/\Delta x + (\rho_{N+1}^t)(x_p - xN)/\Delta x ,$$

and $$P_{xp} = (P_N^t)(x_{N+1} - xp)/\Delta x + (P_{N+1}^t)(xp - xN)/\Delta x .$$

APPENDIX F.--PROGRAM STRUCTURE

Figure F-1 is a flow chart of the program structure. The following abbreviations can be seen in the flow chart:

1. SPTIALC: Used to compute flow field at x_1 and x_2 when $xF^{n+1} = x_1$ $xF^n \leq x_2$.

2. SPTIALO: To compute flow fields at x^{n+1} (open end) when $xF^{n+1} = x_{n+1}$ and $xF^n \geq x_n$.

3. BOUNDRY: To compute flow fields at x_1 and x_{n+1} when flame is at least at a distance of $2\Delta x$ away.

4. ACROSFM: Compute flow fields across flame front.

5. LAXWEND: Compute flow fields by a two-step Lax-Wendroff scheme due to Burstein and Rubin.

6. LINRINT: Linear interpolation routine.

7. QUADINT: Quadratic interpolation routine.

8. MESHONE: To compute flow fields when flame is within the first two meshes.

9. DPMZL, DPMZR, DPMXP: To compute flow fields at the points ZL, ZR, and XP by the method of characteristics.

10. GAMMABU: To estimate γ_b and γ_u.

11. TRANSCL: Compute ρ, m, E from u, P, ρ.

12. TRANSLC: Compute u, P, ρ from ρ, m, E.

Several other functions subprograms such as heat sources and/or sinks Su, ρ_b, E, T_b, γ_u, γ_b, etc., must be supplied by the users.

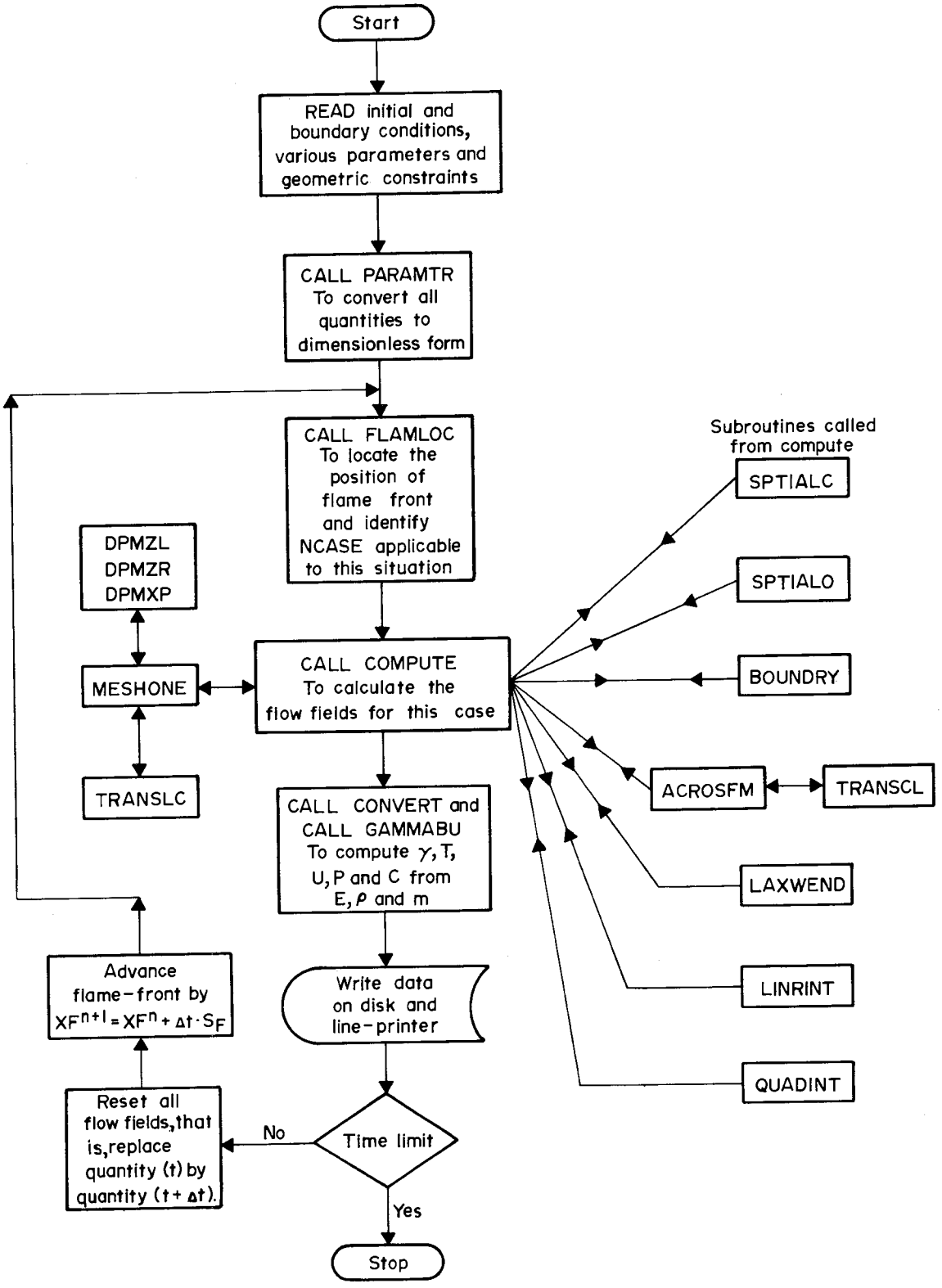

FIGURE F-1. - Program structure.

APPENDIX G.--VISCOUS TERM IN THE ENERGY EQUATION

In the energy equation we should have two terms (41) of the form (considering a two-dimensional case):

$$\text{Exp} = -\vec{\nabla} \cdot \vec{v}P + \vec{\nabla} \cdot (\overleftrightarrow{\pi} \cdot \vec{v})$$

$$= -\left[\frac{\partial uP}{\partial x} + \frac{\partial vP}{\partial y}\right]$$

$$+ \frac{\partial}{\partial x}\left[(\eta u)\frac{\partial u}{\partial x} + (\mu v)\frac{\partial v}{\partial x}\right] + \frac{\partial}{\partial x}\left[(\lambda u)\frac{\partial v}{\partial y} + (\mu v)\frac{\partial u}{\partial y}\right]$$

$$+ \frac{\partial}{\partial y}\left[(\eta v)\frac{\partial v}{\partial y} + (\mu u\ \frac{\partial u}{\partial y}\right] + \frac{\partial}{\partial y}\left[(\lambda v)\frac{\partial u}{\partial x} + (\mu u)\frac{\partial v}{\partial x}\right]$$

where $\lambda = K - \frac{2}{3}\mu$,

$\eta = K + \frac{4}{3}\mu$,

and K = bulk viscosity .

By analyzing the "Assumptions" section, we get

$$\text{Exp} = -\frac{\partial(uP)}{\partial x} + \frac{\partial}{\partial x}\left(\eta u \frac{\partial u}{\partial x}\right) + \frac{\partial}{\partial y}(\mu u)\frac{\partial u}{\partial y} .$$

If L and H are the length and height of an entryway, then

$$\frac{\partial}{\partial x}(uP) = O\left(\frac{uP}{L}\right)$$

and $$\frac{\partial}{\partial x}\left(\eta u \frac{\partial u}{\partial x}\right) + \frac{\partial}{\partial y}\left(\mu u \frac{\partial u}{\partial y}\right) = O\left[\eta \frac{u^2}{L^2} + \mu \frac{u^2}{H^2}\right] .$$

Now we need only to compare

$$P \text{ and } \eta \frac{u}{L} + \frac{u}{H\left(\frac{H}{L}\right)} \approx \mu u \left(\frac{1}{L} + \frac{u}{H(H/L)}\right)$$

$$\leq \mu u \left(\frac{H+L}{H^2}\right) < \mu u \left(\frac{2L}{H^2}\right) .$$

For our problem,

$$\mu \approx 2\times10^{-5} \text{ kg m}^{-1} \text{ sec}^{-1} ,$$

$$H \approx 1 \text{ m} ,$$

$$L \approx 50 \text{ m} ,$$

$$P \approx 1 \text{ atm} = 10^{5} \text{ kg s}^{-2} \text{ m}^{-1} ,$$

and $$u \approx 50 \text{ m} .$$

Then $$P \approx 10^{5}$$

and $$\eta \frac{u}{L} + \mu \frac{u}{H\left(\frac{H}{L}\right)} \leq 10^{-1} .$$

Hence, we simply drop the term $\vec{\nabla} \cdot (\overleftrightarrow{\Pi} \cdot \vec{v})$ from the energy equation.

APPENDIX H.--SYMBOLS LIST

C_v = Constant volume specific heat (m^3 atm K^{-1} g^{-1}).

C_p = Constant pressure specific heat (cal g^{-1} K^{-1}).

C_o = Sound speed in the ambient atmosphere (m sec^{-1}).

C_b = Sound speed on the burned side of the flame front (m sec^{-1}).

C_u = Sound speed on the unburned side of the flame front (m sec^{-1}).

C_+ = The characteristic curve in the +X direction.

C_- = The characteristic curve in the -X direction.

C_g = Particle trajectory.

χ = Expansion ration (= ρ_u / ρ_b).

D = Diameter (m).

Div = Divergence.

d = Hydraulic diameter = 4 X duct area/duct perimeter (m).

E = Total energy per unit volume (atm).

e = Internal energy per unit mass $m^2 sec^{-2}$.

f = Wall friction coefficient (1).

γ_o = A constant rendering the equations nondimentional (= $C_o^2 \rho_o / P_o$).

γ_u = Specific heat ratio on the unburned side (1).

γ_b = Specific heat ratio on the burned side (1).

h = Height of the cross section (m).

L = Width of the cross section (m).

Le = Lewis No. (= $\lambda C_p^{-1} \rho_u^{-1}$).

LT = Length of flame gallery (m).

ℓ = Boundary layer thickness (m).

m = Mass flux $\rho \cdot u$ kg $m^{-2} sec^{-1}$.

μ = Viscosity (kg $m^{-1} sec^{-1}$).

P = Pressure (atm).

P_o = Ambient pressure (atm).

P_u = Pressure on the unburned side of the flame front (atm).

P_b = Pressure on the burned side of the flame front (atm).

PZL = Pressure at the point ZL (atm).

PZR = Pressure at the point ZR (atm).

Qw = Heat loss through the wall per unit mass per unit time ($J\ kg^{-1}\ sec^{-1}$).

Qd = Heat release by coal-dust flame per unit mass per unit time ($J\ kg^{-1}\ sec^{-1}$).

Qr = Heat gain or loss due to radiation ($J\ kg^{-1}\ sec^{-1}$).

Q = Heat transfer per unit mass per unit time ($J\ kg^{-1}\ sec^{-1}$).

R = Universal gas constant ($cm^2\ sec^{-2}\ K^{-1}$).

Ru = R on the unburned side of the flame front.

Rb = R on the burned side of the flame front.

Re = Reynolds number ($= u\ d\ \mu^{-1}\ \rho$).

ρ = Density of gas ($kg\ m^{-3}$).

ρ_u = ρ on the unburned side ($kg\ m^{-3}$).

ρ_b = ρ on the burned side ($kg\ m^{-3}$).

Su = Laminar burning velocity on the unburned side relative to the stationary gas ($m\ sec^{-1}$).

S_b = Laminar burning velocity on the burned side relative to the stationary gas ($m\ sec^{-1}$).

S_f = Flame speed in the laboratory coordinate system ($m\ sec^{-1}$).

St = Stanton number $\left(= \frac{1}{4}\ q\ d[\rho\ C_p\ u\ (T_w - T_o)]^{-1}\right)$.

T = Temperature (K).

T_o = Ambient temperature (K).

T_u = T on the unburned side of the flame front.